

---

# Channelling Multimodality Through a Unimodalizing Transport: Warp-U Sampler and Stochastic Bridge Sampling

Fei Ding,<sup>1,†</sup> David E. Jones,<sup>1,†</sup> Shiyuan He<sup>2</sup> and Xiao-Li Meng<sup>3</sup>

<sup>1</sup>Department of Statistics, Texas A&M University, College Station, 77840, TX, USA

, <sup>2</sup>Institute of Statistics and Big Data, Renmin University of China, Beijing, 100872, China

and <sup>3</sup>Department of Statistics, Harvard University, Cambridge, 02138, MA, USA.

<sup>†</sup>Co-first author.

## Abstract

Monte Carlo integration is fundamental in scientific and statistical computation, but requires reliable samples from the target distribution, which poses a substantial challenge in the case of multi-modal distributions. Existing methods often involve time-consuming tuning, and typically lack tailored estimators for efficient use of the samples. This paper adapts the Warp-U transformation (Wang et al., 2022) to form multi-modal sampling strategy called *Warp-U sampling*. It constructs a stochastic map to transport a multi-modal density into a uni-modal one, and subsequently inverts the transport but with new stochasticity injected. For efficient use of the samples for normalising constant estimation, we propose (i) an unbiased estimation scheme based coupled chains, where the Warp-U sampling is used to reduce the coupling time; and (ii) a stochastic Warp-U bridge sampling estimator, which improves its deterministic counterpart given in Wang et al. (2022). Our overall approach requires less tuning and is easier to apply than common alternatives. Theoretically, we establish the ergodicity of our sampling algorithm and that our stochastic Warp-U bridge sampling estimator has greater (asymptotic) precision per CPU second compared to the Warp-U bridge estimator of Wang et al. (2022) under practical conditions. The advantages and current limitations of our approach are demonstrated through simulation studies and an application to exoplanet detection.

**Key words:** adaptive MCMC, astrostatistics, bridge sampling, Bayesian evidence, multi-modal density, normalising constant estimation.

## 1. Monte Carlo Integration

### 1.1. Computing normalising constants — How hard can it be?

Computing or estimating normalising constants may sound like a routine homework exercise, but it is a surprisingly wide-ranging and hard problem in statistics and more broadly in many scientific applications, from computing the free energy in physics (see Bennett, 1976) to cognitive studies in psychology (see Gronau et al., 2019, 2020). In particular, Bayesian evidence ratios (a.k.a., Bayes factors) are widely used for hypothesis testing and model selection in many scientific fields. For example, Nelson et al. (2020) and Pullen and Morris (2014) discussed the computation of Bayesian evidence in the context of exoplanet detection and systems biology, respectively. Given the many scientific uses of normalising constants, computationally and statistically efficient methods for estimating them are of high practical value, and many powerful algorithms have been (re)invented, as we shall review briefly at the end of this article in Section 6.1. On the other hand, some ubiquitous scenarios remain challenging, such as estimating normalising constants for multi-modal target densities. For example, Nelson et al. (2020) applied numerous strategies for estimating the Bayesian evidence

for the presence of an exoplanet orbiting a star and obtained somewhat divergent estimates, even after substantial calibration efforts.

In general, the problem of computing normalising constants is exceedingly challenging and requires methods tailored to the particular context because if there were an effective generic method for it, then we would have a general efficient method for computing integration, which is impossible with contemporary software, hardware, and *mindware*<sup>1</sup>. Specifically, for any (absolutely integrable) function  $f$  we have

$$\int_{\Theta} f(\boldsymbol{\theta})\mu(d\boldsymbol{\theta}) = \int_{\Theta} f_+(\boldsymbol{\theta})\mu(d\boldsymbol{\theta}) - \int_{\Theta} f_-(\boldsymbol{\theta})\mu(d\boldsymbol{\theta}), \quad (1)$$

where  $\mu$  is a suitable baseline measure<sup>2</sup>, and both  $f_+ = \max\{f(\boldsymbol{\theta}), 0\}$  and  $f_- = -\min\{f(\boldsymbol{\theta}), 0\}$  are non-negative functions and hence can be viewed as un-normalised densities on (possibly a subset of)  $\Theta$ . Consequently, although we will frame our approaches in the context of Monte Carlo estimation of normalising constants, they are generally applicable because of identity (1), and because of other ways of making the integrand positive, such as using a lower bound on  $f$  as a control variate.

We consider the following general problem: for an unnormalised probability density  $q$  with support  $\Theta$ , we seek to estimate the normalising constant  $c = \int_{\Theta} q(\boldsymbol{\theta})\mu(d\boldsymbol{\theta})$ . Any Monte Carlo approach for this problem involves two key tasks: (i) obtaining samples  $\boldsymbol{\theta}_1, \boldsymbol{\theta}_2, \dots, \boldsymbol{\theta}_n$  from  $\pi = q/c$  or some related density (or densities), and (ii) constructing an estimate of  $c$  based on the Monte Carlo samples. These tasks may be performed sequentially or in combination, depending on the specific strategy. It is worth emphasising that when  $\pi$  is multi-modal, substantial inefficiencies can result from not addressing the difficulties created by multi-modality in both (i) and (ii) (on the other hand addressing multi-modality does not automatically guarantee an efficient estimator of  $c$ ).

## 1.2. An Integrated Approach for Combating Multi-modality

We address the multi-modality challenge by an effective Warp-U sampler designed for multi-modal target densities, followed by a complementary strategy for estimating the corresponding target normalising constants. The estimation step is complementary in the sense that much of the necessary computation is completed during the sampling stage. Both our sampling and estimation steps make use of the stochastic Warp-U transformation proposed by Wang et al. (2022), which transforms multi-modal densities into approximately uni-modal ones. The key conceptual step of constructing a Warp-U transformation is to *induce* a mixture representation of the target  $\pi(\boldsymbol{\theta}) = \sum_{k=1}^K w_k \pi_k(\boldsymbol{\theta})$ , where intuitively  $\pi_k$  can be viewed as representing a “sub-population component” that is responsible for the  $k$ th mode in the target density<sup>3</sup>. We will review the construction details in Section 2.1.

The remainder of Section 2 details the sampling step and estimation step of our integrated approach. Section 2.3 develops a Markov chain Monte Carlo (MCMC) sampling algorithm, the *Warp-U sampler*, which alternately applies the stochastic Warp-U transformation and its inverse. The key to this sampler is that the components (i.e. the  $\pi_k$ ’s) of the target are stochastically transported to an intermediate uni-modal density, then the latter gets stochastically transported back to the original target. Since all the target components are mapped to similar intermediate uni-modal densities, the step of mapping back to the target density tends to have a high probability of mapping any given draw to a component different from that which was originally sampled. This property makes the proposed procedure effective for multi-mode exploration, as initially demonstrated in the first version<sup>4</sup> of Wang et al. (2022). Our full algorithm also incorporates a classical

<sup>1</sup> A term coined by psychologist David Perkins, referring to the knowledge and problem solving techniques available to human minds.

<sup>2</sup> See Kong et al. (2003) for the essential role the baseline measure  $\mu$  plays in forming an appropriate likelihood theory for Monte Carlo integration.

<sup>3</sup> It is worthwhile, however, to remind ourselves that the relationship between multi-modality and mixture distributions is a lose one. For example, a mixture distribution can easily exhibit a single mode when the mixture components are sufficiently close to each other.

<sup>4</sup> See Section 6 of the initial version at <https://arxiv.org/pdf/1609.07690v1.pdf>, which was removed in the published version, following an editorial request to streamline Wang et al. (2022).

Metropolis-Hastings update to ensure irreducibility, and our simulation results given in Section 4 demonstrate that it can be substantially more efficient than competing approaches for sampling from multi-modal targets, such as parallel tempering (Geyer, 1991).

The quality of the Warp-U transformation obviously affects the convergence behaviour of the Warp-U sampler. In the estimation strategy proposed by Wang et al. (2022), a Gaussian mixture approximation is fit to the target density  $\pi$ , which is then used to build a Warp-U map. But in the sampling context, initially there are no Monte Carlo samples with which to fit any kind of mixture. To address this issue, we adopt an adaptive Warp-U sampler which starts by sampling from a uniform density, or any other over-dispersed crude approximation to the target density, and then proceeds in stages, updating the approximating density at each stage. Importantly, as with the Warp-U bridge sampling estimation strategy of Wang et al. (2022), it is unnecessary for the approximating density to be a precise representation of the target density in order to substantially improve MCMC convergence speed; any reasonable approximation is sufficient to generate practically meaningful acceleration. This means that the number of stages needed in our algorithm is typically small, e.g., fewer than ten. Later in Section 3.1, we prove that the adaptive Warp-U sampler is ergodic, following the approach of Roberts and Rosenthal (2007).

Given MCMC samples from  $\pi$ , we are often interested in estimating  $\mathbb{E}_\pi h(\boldsymbol{\theta})$  for a chosen function  $h$ , where the expectation is taken with respect to  $\boldsymbol{\theta} \sim \pi$ . Traditional methodology requires running a long Markov chain and performing convergence diagnostics to guarantee accurate estimation. In Section 2.4, we devise an unbiased estimation strategy for the Warp-U sampler, follow the strategy proposed and tested by Jacob et al. (2020). The advantage of this unbiased approach is its direct assessment of chain convergence, both theoretically and practically, through the  $L$ -coupling method, as elaborated in Biswas et al. (2019), and further investigated in Craiu and Meng (2022). Under this scheme, two Warp-U sampling chains run concurrently and are prompted to meet. In particular, we use optimal transport coupling to keep the two chains close during their transitions between density modes. This implementation ensures that we obtain genuinely unbiased moment estimates under multi-modal distributions, regardless of the isolation of the density modes.

As another key ingredient to our estimation step, Section 2.5 proposes a divide-and-conquer strategy to break a computational bottleneck that appears in the Warp-U bridge estimators of Wang et al. (2022). Warp-U bridge estimators apply standard bridge sampling estimators (Bennett, 1976; Meng and Wong, 1996) to the (approximately) uni-modal  $\tilde{q}$  resulting from the Warp-U transformation, which preserves the normalising constant, i.e.,  $\int_{\Theta} \tilde{q}(\boldsymbol{\theta})\mu(d\boldsymbol{\theta}) = c = \int_{\Theta} q(\boldsymbol{\theta})\mu(d\boldsymbol{\theta})$ . The bottleneck is created by the large number of ‘‘cross-component’’ function evaluations needed for implementing bridging sampling estimators using  $\tilde{q}$  and all the Warp-U transformed draws. In Section 3.2 we prove that, in comparison with the Warp-U bridge estimator, a substantial reduction in asymptotic variance can be obtained by instead applying standard bridge sampling to estimate the normalising constant of each mixture component  $q_k = c\pi_k$ , for  $k = 1, \dots, K$ , and then combining the results to estimate  $c$ . The simulation studies reported in Section 4.3 show that, *given fixed computational resources*, this divide-and-conquer approach incurs substantially lower root mean squared error (RMSE) than the corresponding ones given in Wang et al. (2022).

In Section 5, we apply our integrated approach to estimating the Bayesian evidence for exoplanets based on radial velocity (RV) data, which demonstrates its potential for outperforming existing sampling and estimation strategies applied together in various combinations, including combining parallel tempering with the Warp-U bridge estimator of Wang et al. (2022). In order to report our main proposals as soon as possible, we defer the literature review to Section 6, where we also discuss the limitations of our approach and possible improvements and extensions, such as how the divide-and-conquer method might be combined with the unbiased estimation strategy to reduce both variance and bias. Proofs are given in the online Supplementary Material.

## 2. Warp-U Sampling and Estimation Methods

### 2.1. Bridge Sampling Estimation and Warp-U Transformations

Let  $q_1$  and  $q_2$  denote unnormalised densities with unknown normalising constants  $c_1$  and  $c_2$ , respectively, and for simplicity we assume they share the same support  $\Theta = \mathbb{R}^d$ . We are interested in estimating their ratio  $r = c_1/c_2$  (e.g., a Bayes factor). For this scenario, bridge sampling (Bennett, 1976; Meng and Wong, 1996)

relies on the following identity:

$$r = \frac{c_1}{c_2} = \frac{\mathbb{E}_{p_2}[q_1(\boldsymbol{\theta})\alpha(\boldsymbol{\theta})]}{\mathbb{E}_{p_1}[q_2(\boldsymbol{\theta})\alpha(\boldsymbol{\theta})]}, \quad (2)$$

where  $\alpha$  is the bridge function (discussed below), and  $\mathbb{E}_{p_i}$  denotes an expectation with respect to  $\boldsymbol{\theta} \sim p_i = q_i/c_i$ , for  $i = 1, 2$ . This identity leads naturally to the bridge sampling estimator:

$$\hat{r} = \frac{n_2^{-1} \sum_{j=1}^{n_2} q_1(\boldsymbol{\theta}_{2,j})\alpha(\boldsymbol{\theta}_{2,j})}{n_1^{-1} \sum_{j=1}^{n_1} q_2(\boldsymbol{\theta}_{1,j})\alpha(\boldsymbol{\theta}_{1,j})}, \quad (3)$$

where  $\{\boldsymbol{\theta}_{i,1}, \dots, \boldsymbol{\theta}_{i,n_i}\}$  are (possibly dependent) samples from  $p_i$ , and  $n_i$  is the number of samples from  $q_i$ , for  $i = 1, 2$ . When the samples are independent, Meng and Wong (1996) showed that the optimal  $\alpha$  is

$$\alpha_r(\boldsymbol{\theta}) \propto [s_1 q_1(\boldsymbol{\theta}) + r s_2 q_2(\boldsymbol{\theta})]^{-1}, \quad (4)$$

where  $s_i = n_i/(n_1 + n_2)$  ( $i = 1, 2$ ), in the sense that this choice yields the smallest asymptotic variance for the estimator  $\hat{r}$ . As expected, the unknown  $r$  appears in the optimal choice of  $\alpha$ , but this issue can be easily addressed by introducing an iterative scheme  $\{r^{(t)}, t = 1, \dots\}$ , where  $r^{(t)}$  is given by (3) with  $\alpha = \alpha_{r^{(t-1)}}$ . This approach was proposed by Meng and Wong (1996) who showed that  $\lim_{t \rightarrow \infty} r^{(t)}$  maintains the asymptotic variance of the optimal bridge sampling estimator for  $r$  that uses the true value of  $r$  in  $\alpha_r$ .<sup>5</sup>

In some cases, there is only one unnormalised density  $q = c\pi$ , but bridge sampling is still applicable, and indeed preferred. We can set  $q_1 = q$  in (3), and then have the freedom to choose the ‘‘pairing’’ density  $q_2 = p_2$  to be any normalised density (i.e.,  $c_2 = 1$ ), such as a Gaussian distribution. When we are interested in estimating (ratios of) many normalising constants, we can choose to apply bridge sampling to them simultaneously, or separately by judiciously choosing a pairing density for each (or some) of them (Meng and Schilling, 2002). The choice of  $p_2$  is important because the asymptotic variance of  $\hat{c}$  decreases as the separation between  $p_1 = \pi$  and  $p_2$  decreases. Their separation is measured by the sample-size adjusted harmonic divergence

$$H_A(p_1, p_2) = 1 - \int [\eta_1 p_1^{-1}(\boldsymbol{\theta}) + \eta_2 p_2^{-1}(\boldsymbol{\theta})]^{-1} \mu(d\boldsymbol{\theta}), \quad (5)$$

where  $\eta_i \propto s_i^{-1}$ . Obviously,  $p_2(\boldsymbol{\theta})$  should also be chosen to minimise computation in terms of both function evaluation and sampling.

Given the above considerations, if  $\pi = q/c$  is multi-modal, it is natural to choose  $p_2$  to be a Gaussian mixture distribution approximating  $\pi$ , i.e.,

$$\phi_{\text{mix}}(\boldsymbol{\theta}) = \sum_{k=1}^K \phi^{(k)}(\boldsymbol{\theta}) = \sum_{k=1}^K w_k |\mathcal{S}_k^{-1}| \phi(\mathcal{S}_k^{-1}(\boldsymbol{\theta} - \boldsymbol{\mu}_k)), \quad (6)$$

where  $w_k$ ,  $\boldsymbol{\mu}_k$ , and  $\mathcal{S}_k$  denote a weight, mean vector, and scale matrix, respectively, and  $\phi$  is the density of  $\mathcal{N}_d(\mathbf{0}, \mathbf{I})$ . In (6) and throughout, we use  $\phi^{(k)}$  to denote the  $k$ -th component of  $\phi_{\text{mix}}$  including its mixture weight  $w_k$ . Standard bridge sampling estimation would proceed by applying (3) with densities  $q_1 = q$  (unnormalised) and  $q_2 = \phi_{\text{mix}}$ . The top left panel of Figure 1 provides an illustrative example in which  $\phi_{\text{mix}}$  (dashed curve) is a three component Gaussian mixture and roughly approximates  $\pi$  (solid curve). In general, the quality of the approximation affects the accuracy of the estimator  $\hat{r}$  in (3).

Wang et al. (2022) proposed an improved approach called Warp-U bridge estimation based on the idea of warp bridge sampling estimation (Meng and Schilling, 2002). By the properties of  $f$ -divergences (Ali and Silvey, 1966), for which the Harmonic diverge of (5) is a special case, any transformation  $\mathcal{F}$  will not increase the divergence between  $\pi$  and  $\phi_{\text{mix}}$ , i.e.,  $H_A(\pi, \phi_{\text{mix}}) \geq H_A(\mathcal{F}(\pi), \mathcal{F}(\phi_{\text{mix}}))$ . Since the asymptotic variance

<sup>5</sup> This turns out to be a consequence of the fact that the fix-point equation implied by (3)-(4) is equivalent to the score equation for the maximum likelihood estimator of  $r$  from the likelihood theory (for Monte Carlo integration) as formulated in Kong et al. (2003), and hence the adaption does not lead to loss of information, at least asymptotically.

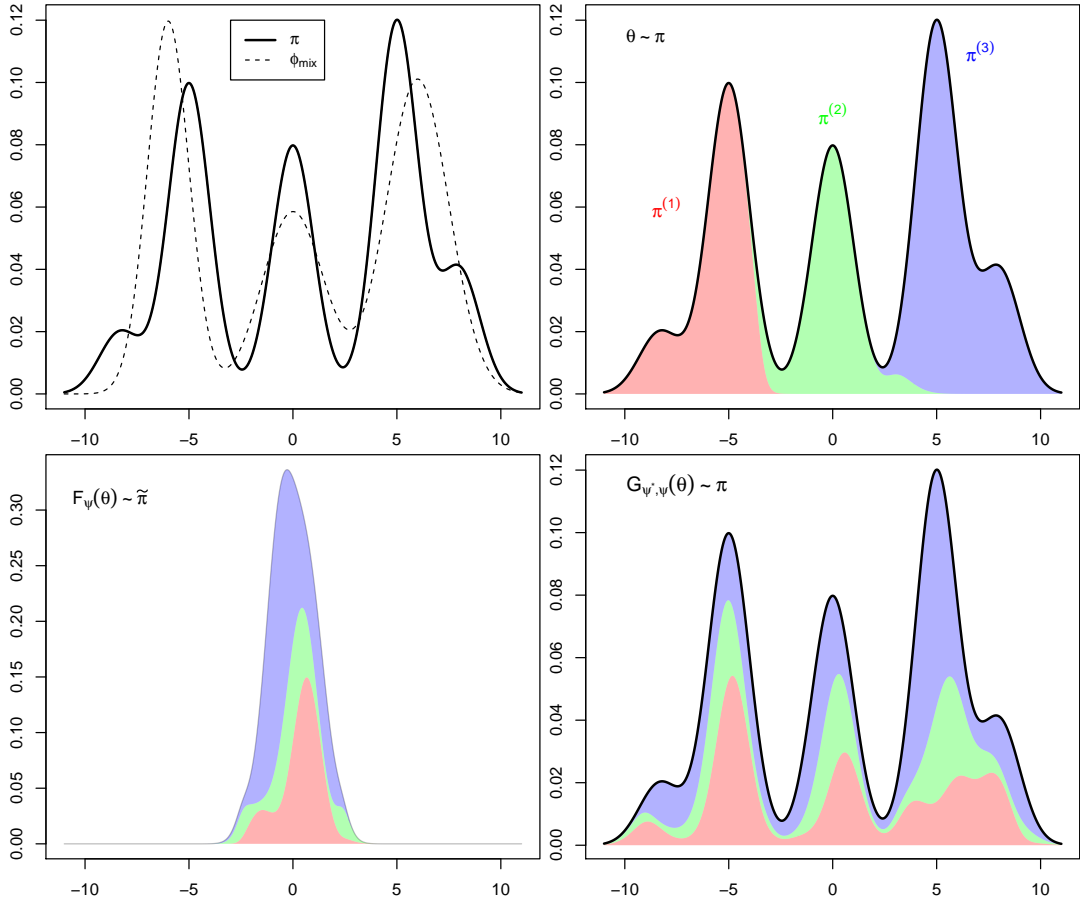


Fig. 1: Top left: the Gaussian mixture  $\phi_{\text{mix}}$  (dashed line) is a rough approximation to the target density  $\pi$  (solid line). Top right: the components  $\pi^{(1)}$ ,  $\pi^{(2)}$ , and  $\pi^{(3)}$  of  $\pi$  sliced by  $\phi_{\text{mix}}$  are shown as red, green and blue regions, respectively. Bottom left: the transformed density  $\tilde{\pi}$  obtained by applying the stochastic Warp-U transformation  $\mathcal{F}_\psi$ . Bottom right: applying  $\mathcal{G}_{\psi',\psi} = \mathcal{H}_{\psi'} \circ \mathcal{F}_\psi$  (i.e., the Warp-U transformation and its inverse) exactly recovers the original  $\pi$  (black solid line); the shaded colours indicate the proportion of density transported from the original components of  $\pi$ .

---

**Algorithm 1** Warp-U estimation of  $c$  (Wang et al., 2022)

**Inputs:** samples  $\theta_{1,1}, \dots, \theta_{1,n_1} \sim \pi$  and  $\theta_{2,1}, \dots, \theta_{2,n_2} \sim \phi$ , and parameters  $w_k, S_k, \mu_k$  for  $k = 1, \dots, K$ , see (6).

- 1: Set  $\theta_{1,j}^* = \mathcal{F}_{\psi_j}(\theta_{1,j}) = \mathcal{S}_{\psi_j}^{-1}(\theta_{1,j} - \mu_{\psi_j})$  with  $\psi_j$ 's independently drawn from (7) for  $j = 1, \dots, n_1$ .
  - 2: Apply (3) using the densities  $q_1 = \tilde{\pi}$  in (8) and  $q_2 = \phi$ , and the samples  $\theta_{1,j}^*, \dots, \theta_{1,n_1}^* \sim \tilde{\pi}$  (from Step 1) and  $\theta_{2,1}, \dots, \theta_{2,n_2} \sim \phi$  (from the inputs).
- 

of  $\hat{r}$  decreases with the divergence (5), a transformation of the densities will generally decrease the asymptotic variance, as long as the transformation does not alter the underlying normalising constant. In many cases, a good choice of  $\mathcal{F}$  can provide substantial efficiency gains.

Given all the desirable properties discussed above, a natural choice of transformation would be the *distributional normalisation*:  $\theta^* = \mathcal{F}_\psi(\theta) := \mathcal{S}_\psi^{-1}(\theta - \mu_\psi)$ , where the index  $\psi \in \{1, \dots, K\}$  is drawn from

$$\varpi(\psi|\theta) = \frac{\phi^{(\psi)}(\theta)}{\phi_{\text{mix}}(\theta)}. \quad (7)$$

This conditional distribution is the weight of the  $\psi$ -th component of  $\phi_{\text{mix}}$  at  $\theta$ . When  $\theta \sim \phi_{\text{mix}}$  and  $\psi$  is sampled from (7),  $\mathcal{F}_\psi(\theta) \sim \mathcal{N}_d(\mathbf{0}, \mathbf{I})$ . That is, in addition to the usual normalisation that renders mean zero and variance one, the stochastic map  $\mathcal{S}_\psi$  *normalises*  $\phi_{\text{mix}}$  in distribution, since it becomes  $\mathcal{N}_d(\mathbf{0}, \mathbf{I})$ . This is the Warp-U transformation given in Wang et al. (2022).

Since  $\phi_{\text{mix}}$  approximates  $\pi$ , it is intuitive that applying the stochastic Warp-U transformation to  $\pi$  (with  $\theta \sim \pi = cq$  and  $\psi \sim \varpi(\psi|\theta)$ ) also gives an approximately uni-modal density. The transformed version of  $q$  is given by

$$\tilde{q}(\theta^*) = \sum_{k=1}^K \phi(\theta^*) \frac{q(\mathcal{S}_k \theta^* + \mu_k)}{\phi_{\text{mix}}(\mathcal{S}_k \theta^* + \mu_k)} w_k. \quad (8)$$

Wang et al. (2022) show that  $\tilde{q}$  maintains the same normalising constant as  $q$ , and hence we can apply bridge sampling to  $\tilde{q}$  for estimating  $c$ , as detailed in Algorithm 1.

To visualise (8), the coloured regions in the top right panel of Figure 1 show the components  $\pi^{(k)}(\theta) = \varpi(k|\theta)\pi(\theta)$  (as functions of  $\theta$ ) of  $\pi$  (black solid curve) induced by  $\phi_{\text{mix}}$  (the dashed curve in the top left panel). The density of  $\pi^{(k)}$  gets transported towards the origin via the mapping  $\mathcal{F}_\psi$  with  $\psi = k$ . The bottom left panel of Figure 1 is the resulting Warp-U transformed density  $\tilde{\pi}$ . The shaded regions represent the proportion of density contributed from the original components of  $\pi$  with the corresponding colours.

## 2.2. A Distribution-Preserving Mass-swapping Transport

Recall that, when  $\theta \sim \pi$ , the Warp-U transformed random variable  $\theta^* = \mathcal{F}_\psi(\theta)$  follows  $\tilde{\pi} = \tilde{q}/c$ , where  $\tilde{q}$  is given by (8). The essence of our Warp-U sampler is to additionally apply the *inverse* Warp-U transformation to obtain a draw  $\theta'$  that follows the original target density  $\pi$ . That is, we set  $\theta' = \mathcal{H}_{\psi'}(\theta^*) := \mathcal{F}_{\psi'}^{-1}(\theta^*) = \mathcal{S}_{\psi'}\theta^* + \mu_{\psi'}$ , where the random index  $\psi'$  is generated to be generally different from  $\psi$  but preserves  $\theta' \sim \pi$ . We can achieve this easily and in general once we notice that as long as  $\mathcal{F}_\psi$  is bijective given  $\psi$ , we have

$$\theta = \mathcal{F}_\psi^{-1}(\theta^*), \quad \text{and} \quad \theta' = \mathcal{F}_{\psi'}^{-1}(\theta^*) \quad (9)$$

by construction. This parallel expression immediately establishes the following general result, which applies to any bijective  $\mathcal{F}_\psi$  (e.g., it does not need to be a Warp-U transformation) and any stochastic index  $\psi$  (e.g., it does not need to be discrete).

**Theorem 1** *Let  $\theta^* = \mathcal{F}_\psi(\theta)$  be a stochastic map from  $\Theta$ , the support of a random variable  $\theta$ , to itself, where the index  $\psi$  is a random variable which has a well-defined joint distribution with  $\theta$ . Suppose  $\mathcal{F}_\psi(\cdot)$  is bijective for any given value of  $\psi$ . Let  $\psi'$  be a random draw from  $\nu(\psi|\theta^*)$ , the conditional distribution of  $\psi$  given  $\theta^*$ , as implied by the joint distribution of  $(\psi, \theta)$ . Then  $\theta' = \mathcal{F}_{\psi'}^{-1}(\mathcal{F}_\psi(\theta))$  and  $\theta$  are identically distributed. Furthermore, if  $\psi'$  and  $\psi$  are independent conditional on  $\theta^*$ , then  $\theta'$  and  $\theta$  are i.i.d. given  $\theta^*$ .*

Consequently, by drawing  $\psi'$  independently from

$$\nu(\psi|\theta^*) \propto \varpi(\psi|\theta = \mathcal{H}_\psi(\theta^*))q(\mathcal{H}_\psi(\theta^*)) \times |\mathcal{H}'_{\psi'}(\theta^*)|, \quad (10)$$

where  $|\mathcal{H}'_{\psi'}(\theta^*)|$  is the Jacobian of  $\mathcal{F}_{\psi'}^{-1}$ , we not only ensure  $\mathcal{G}_{\psi', \psi} = \mathcal{H}_{\psi'} \circ \mathcal{F}_\psi$  is distribution preserving, but also that its output  $\theta'$  is conditionally independent of  $\theta$  given  $\theta^*$ . This conditional independence, which holds regardless of the distribution of  $\theta^*$ , is critical for preventing our algorithm from being trapped by any particular mode, statistically speaking. Note that neither the distribution preserving property nor the conditional independence requires knowledge of how well  $\phi_{\text{mix}}$  approximates  $\pi$ .

**Algorithm 2** Basic Warp-U MCMC sampler

**Input:** parameters  $K$  and  $w_k, S_k, \mu_k$ , for  $k = 1, \dots, K$ , see (6), proposal variance  $\sigma^2$ , initial value  $\theta_0$ , and number of samples to be collected  $T$ .

- 1: **for**  $t = 1, 2, \dots, T$  **do**
- 2: (i) Generate  $\theta^{\text{MH}}$  using a Metropolis-Hasting step with proposal  $\mathcal{N}(\theta_{t-1}, \sigma^2 \mathbf{I})$ .
- 3: (ii) Sample  $\psi$  from  $\varpi(\psi|\theta^{\text{MH}}) = \phi^{(\psi)}(\theta^{\text{MH}})/\phi_{\text{mix}}(\theta^{\text{MH}})$ .
- 4: (iii) Set  $\theta^* = \mathcal{F}_\psi(\theta^{\text{MH}})$ , where  $\mathcal{F}_\psi(\theta^{\text{MH}}) = \mathcal{S}_\psi^{-1}(\theta^{\text{MH}} - \mu_\psi)$ .
- 5: (iv) Sample  $\psi'$  from  $\nu(\psi'|\theta^*) \propto \varpi(\psi'|\mathcal{H}_{\psi'}(\theta^*))q(\mathcal{H}_{\psi'}(\theta^*))|\mathcal{H}'_{\psi'}(\theta^*)|$ .
- 6: (v) Set  $\theta_t = \mathcal{H}_{\psi'}(\theta^*) = \mathcal{S}_{\psi'}\theta^* + \mu_{\psi'}$ .
- 7: **end for**

The bottom right panel of Figure 1 illustrates the result of the two-step stochastic transformation  $\mathcal{G}_{\psi', \psi} = \mathcal{H}_{\psi'} \circ \mathcal{F}_\psi$  applied to  $\pi$ , using the  $\phi_{\text{mix}}$  in the top left panel. The transformation exactly recovers the original density  $\pi$  (the solid black curve). More importantly, the transformation swaps probability masses among the original components of  $\pi$ , which are coloured in the top right panel. In the bottom right panel of Figure 1, the shaded regions indicate the proportion of density contributed from each original component of  $\pi$  with the corresponding colour. At most  $\theta$  locations, there is a considerable amount of density transported from each of the original components of  $\pi$ . A significant consequence is that by repeatedly applying the random transformation  $\mathcal{G}$  to  $\pi$  the mass between its components gets quickly mixed.

Here the transported masses are calculated in the following way. Let

$$\pi_{\psi', \psi}(\theta) = \pi(\mathcal{G}_{\psi', \psi}^{-1}(\theta)) \times |(\mathcal{G}_{\psi', \psi}^{-1})'(\theta)| \times p(\psi', \psi|\mathcal{G}_{\psi', \psi}^{-1}(\theta)), \quad (11)$$

where  $|(\mathcal{G}_{\psi', \psi}^{-1})'(\theta)|$  is the Jacobian of  $\mathcal{G}_{\psi', \psi}^{-1}$ , and  $p(\psi', \psi|\xi) = \varpi(\psi|\xi) \times \nu(\psi'|\mathcal{F}_\psi(\xi))$  is the probability of choosing the transformation  $\mathcal{G}_{\psi', \psi}$  at  $\theta = \xi$  (with  $\theta$  being generic notation), that is, the probability of selecting  $\psi$  and transitioning to  $\psi'$ . Then by applying Theorem 1 with discrete index  $\psi$ , we have

$$\pi(\theta) = \sum_{\psi=1}^K \sum_{\psi'=1}^K \pi_{\psi', \psi}(\theta), \quad (12)$$

because Theorem 1 tells us that averaging over all the possible transitions must recover  $\pi$ , since  $\theta$  and  $\theta'$  have the same distribution. Therefore, the function

$$f^{(\psi)}(\theta) = \sum_{\psi'=1}^K \pi_{\psi', \psi}(\theta) \quad (13)$$

can be interpreted as the amount of density transported or redistributed<sup>6</sup> from the  $\psi$ -th original component of  $\pi$ . The densities  $f^{(\psi)}(\theta)$ ,  $\psi = 1, 2, 3$  correspond to the three shaded areas with different colours in the bottom right panel of Figure 1.

### 2.3. A Warp-U Sampler

The redistribution of masses via Warp-U transformations provides a candidate MCMC sampler. Given one initial sample  $\theta_0$ , we can repeatedly apply the random transformation  $\theta_t = \mathcal{G}_{\psi', \psi}(\theta_{t-1})$  to generate a sequence of  $\theta$ 's which switches among the target components. However, this switching is not quite sufficient to construct a valid MCMC sampler, because the resulting Markov chain is not guaranteed to be irreducible

<sup>6</sup> Note that this redistribution includes the term  $\pi_{\psi, \psi}(\theta)$ .

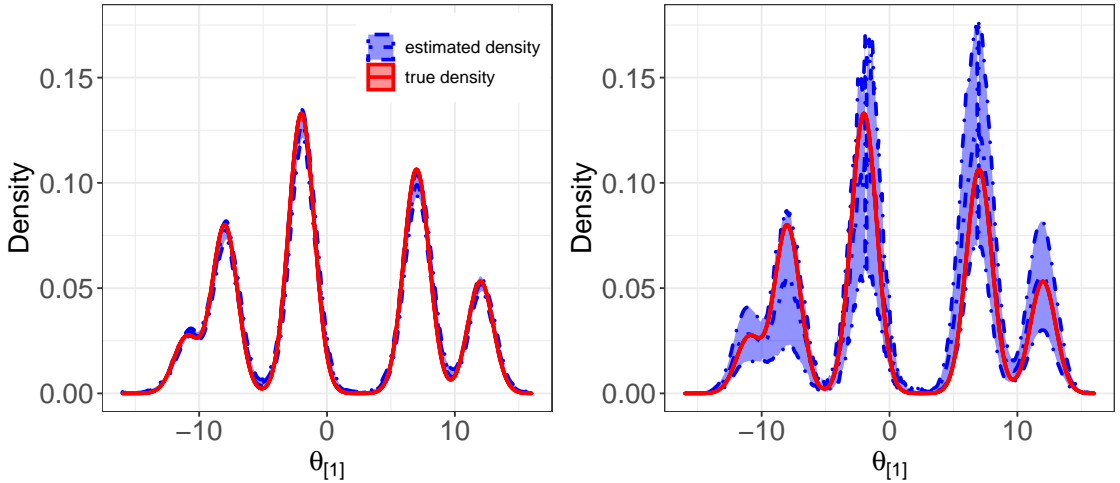


Fig. 2: One marginal of the true target density (solid red line) and the estimated density (centre dash-dot blue line) obtained by running Algorithm 2. The left and right panels show the case where  $\phi_{\text{mix}}$  is set to be the target density and a two Gaussian mixture approximation, respectively. The shaded blue regions indicate pointwise 95% confidence intervals.

in general. For illustration, consider an example where the auxiliary distribution (6) is set as

$$\phi_{\text{mix}}(\boldsymbol{\theta}) = \sum_{k=1}^K \phi(\boldsymbol{\theta} - \boldsymbol{\mu}_k) / K. \quad (14)$$

In this case, each  $\mathcal{G}_{\psi', \psi}(\boldsymbol{\theta}) = \boldsymbol{\theta} - \boldsymbol{\mu}_{\psi'} + \boldsymbol{\mu}_{\psi}$  is a shift transformation. Given the initial  $\boldsymbol{\theta}_0$ , the subsequent sequence  $\boldsymbol{\theta}_t$  can only visit the set

$$\Theta = \{\boldsymbol{\theta} : \boldsymbol{\theta} = \boldsymbol{\theta}_0 + j_1 \boldsymbol{\mu}_1 + \cdots + j_K \boldsymbol{\mu}_K, j_1, \dots, j_K \in \mathbb{Z}\}.$$

where  $\mathbb{Z}$  is the set of all integers. The set  $\Theta$  is a countable grid in  $\mathbb{R}^d$ , and the minimal spacing between the grid points is  $\min_{k \neq k'} \|\boldsymbol{\mu}_k - \boldsymbol{\mu}_{k'}\|_2$ . When the target  $\pi$  has a (continuous) compact support set  $\Omega$ , the chain can only move among a finite number of candidates inside  $\Omega \cap \Theta$ , and hence it cannot converge to the target density for any starting value  $\boldsymbol{\theta}_0$ .

This issue is fully resolved by introducing a Metropolis-Hasting (MH) step between consecutive  $\mathcal{G}_{\psi', \psi}$  transformations. Algorithm 2 specifies the basic version of our Warp-U MCMC sampler. The algorithm proceeds by executing a random walk MH step at the beginning of each iteration followed by the stochastic transformations  $\mathcal{F}_{\psi}$  and  $\mathcal{F}_{\psi'}^{-1}$  with random indices  $\psi, \psi'$ . The ergodicity of this MCMC sampler will be verified in Section 3.1. It is worth noting that the proposed sampler is still valid if the MH step in Line 2 of Algorithm 2 is replaced by other samplers, e.g., the Metropolis adjusted Langevin or Hamiltonian Monte Carlo samplers.

The performance of Algorithm 2 depends on the quality of the approximation  $\phi_{\text{mix}}$ . Figure 2 shows an example where samples obtained via Algorithm 2 are employed to recover one marginal of a four-dimensional target density  $\pi$ . The true density  $\pi$  is a mixture of Gaussian distributions specified by (S.1) in Section S.1 of the online Supplementary Material. The left panel of Figure 2 shows the true density (solid red line) and estimated density (centre dash-dot blue line) in the case where  $\phi_{\text{mix}}$  is the true target  $\pi$ . The right panel shows the case where  $\phi_{\text{mix}}$  is a two-mode Gaussian mixture distribution given by (S.4) in Section S.1. The blue regions show pointwise 95% confidence regions obtained by running Algorithm 2 fifty times with the same initial value and  $T = 3,000$  and then applying the kernel density estimation function `density` in R to



**Algorithm 3** Adaptive Warp-U MCMC sampler

- 
- Input:** proposal variance  $\sigma^2$ , initial value  $\theta_0$ , number of within stage samples  $T$ .
- 1: Obtain  $T$  samples  $\Theta_0$  from the uniform density with support  $\Theta$  (or another initial density with support  $\Theta$ ).
  - 2: Compute  $\phi_{\text{mix}}^{(0)}$  by fitting  $\phi_{\text{mix}}$  using the samples  $\Theta_0$  from Step 1.
  - 3: **for**  $s = 1, 2, \dots, M$  **do**
  - 4: (i) Apply Algorithm 2 with the following inputs: the parameters of  $\phi_{\text{mix}}^{(s-1)}$ ,  $\sigma^2$ ,  $\theta_0$ , and  $T$ . Thus obtain new samples  $\Theta_{\text{new}}$ . Then set  $\Theta_s = \Theta_{s-1} \cup \Theta_{\text{new}}$ .
  - 5: (ii) With probability  $p_s$ , obtain  $\phi_{\text{mix}}^{(s)}$  by re-fitting  $\phi_{\text{mix}}$  using the samples  $\Theta_s$  from Step 4, otherwise set  $\phi_{\text{mix}}^{(s)} = \phi_{\text{mix}}^{(s-1)}$ .
  - 6: **end for**
- 

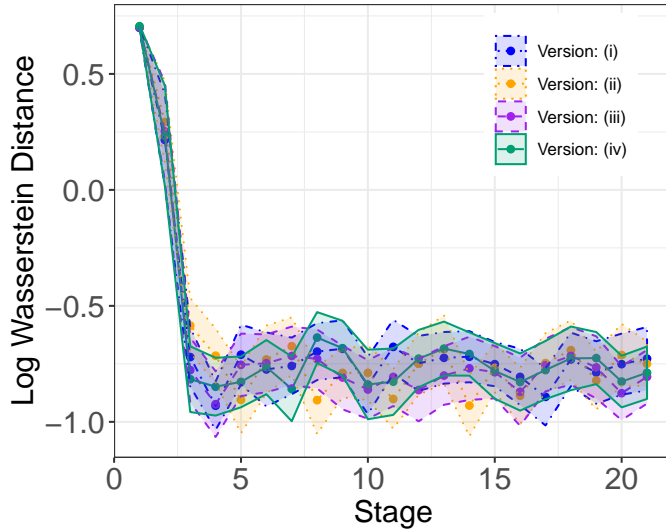


Fig. 3: Log Wasserstein distance between the true target density (see (S.1) in Section S.1 of the online Supplementary Material) and a kernel density estimate computed from samples generated via four versions of Algorithm 3, against the stage number of Algorithm 3. The four algorithm versions are described in the main text and Table 1.

each set of the 3,000 samples obtained. In both panels, the confidence regions approximately cover the true density, but as expected, the uncertainty region is much narrower in the left panel where the underlying  $\phi_{\text{mix}}$  is a closer (exact) approximation to  $\pi$ . Note that we deliberately did not impose any burn-in period in order to measure the quality of the algorithms in their entirety.

In order to make our Warp-U MCMC sampler less dependent on the quality of  $\phi_{\text{mix}}$ , we introduce an adaptive version in Algorithm 3, which performs a periodic update of  $\phi_{\text{mix}}$ . In particular, Algorithm 3 adopts the strategy of using increasingly rare updates (Chimisso et al., 2018; Pompe et al., 2020). After each round of  $T$  iterations of Algorithm 2, Algorithm 3 updates  $\phi_{\text{mix}}$  from the accumulated samples  $\Theta_s$  with probability  $p_s$ , where  $\lim_{s \rightarrow \infty} p_s = 0$ . (We adopt  $p_s = e^{1-s^{1/8}}$  in the numerical sections, but it is important to note that any  $p_s$  satisfying the condition  $\lim_{s \rightarrow \infty} p_s = 0$  can be employed.) This strategy guarantees the ergodicity of the algorithm while at the same time allowing the component number  $K$  in  $\phi_{\text{mix}}$  to gradually increase when needed in order to approximate highly multi-modal  $\pi$ .

In our numerical studies, we implement the EM algorithm to update  $\phi_{\text{mix}}$  based on the accumulated samples  $\Theta_s$ . The complexity of updating the Gaussian mixture approximation  $\phi_{\text{mix}}$  is  $\mathcal{O}(t_{\text{max}} K T s)$ , where

**Table 1.** Four versions of Algorithm 3.

	Step 5 not skipped	Step 5 skipped for $s > 10$
Step 5 using all samples	(i)	(ii)
Step 5 using randomly selected samples	(iii)	(iv)

**Algorithm 4** Warp-U Sampler with Unbiased Estimator

- 1: Sample  $\theta_{1,0}, \theta_{2,0}$  from some initial distribution  $\pi_0$ .
- 2: Generate  $\theta_1^{\text{MH}}$  using a Metropolis-Hasting step with proposal  $\mathcal{N}(\theta_{1,0}, \sigma^2 \mathbf{I})$ .
- 3: Set  $\theta_1^* = \mathcal{F}_{\psi_1}(\theta_1^{\text{MH}})$ , where  $\psi_1 \sim \varpi(\psi_1 | \theta_1^{\text{MH}})$ .
- 4: Set  $\theta_{1,1} = \mathcal{H}_{\psi'_1}(\theta_1^*)$  where  $\psi'_1 \sim \nu(\psi'_1 | \theta_1^*)$ .
- 5: **for**  $t = 2, 3, \dots, T$  **do**
- 6:   Generate  $\theta_1^{\text{MH}}, \theta_2^{\text{MH}}$  jointly using a Metropolis-Hasting step with maximal coupling (or reflection coupling). The marginals of the joint proposal are  $\mathcal{N}(\theta_{1,t-1}, \sigma^2 \mathbf{I})$  and  $\mathcal{N}(\theta_{2,t-2}, \sigma^2 \mathbf{I})$ .
- 7:   Set  $\theta_1^* = \mathcal{F}_{\psi_1}(\theta_1^{\text{MH}})$  and  $\theta_2^* = \mathcal{F}_{\psi_2}(\theta_2^{\text{MH}})$ , where  $(\psi_1, \psi_2)$  are sampled with optimal transport coupling with marginals  $\varpi(\psi_1 | \theta_1^{\text{MH}})$  and  $\varpi(\psi_2 | \theta_2^{\text{MH}})$ .
- 8:   Set  $\theta_{1,t} = \mathcal{H}_{\psi'_1}(\theta_1^*)$  and  $\theta_{2,t-1} = \mathcal{H}_{\psi'_2}(\theta_2^*)$  where  $(\psi'_1, \psi'_2)$  are sampled with optimal transport coupling with marginals  $\psi'_1 \sim \nu(\psi'_1 | \theta_1^*)$  and  $\psi'_2 \sim \nu(\psi'_2 | \theta_2^*)$ .
- 9: **end for**
- 10: Compute  $H_{l,m}(\theta_{1,\cdot}, \theta_{2,\cdot})$  in (17).

$t_{\max}$  is the maximum number of iterations of the EM algorithm, and  $s$  is the current stage number of Algorithm 3. In practice, to save computational resources, instead of using all  $sT$  samples of  $\Theta_s$  to update  $\phi_{\text{mix}}$  in Step 5 of Algorithm 3, we can use  $T$  samples randomly selected from  $\Theta_s$ . Alternatively, the update of  $\phi_{\text{mix}}$  can be eventually stopped, e.g., once  $s > 10$ . Figure 3 shows the log Wasserstein distance between the true target density and a kernel density estimate computed from samples generated via the following four versions of Algorithm 3: (i) Algorithm 3 as written above (dash-dot blue line), (ii) Step 5 is skipped for  $s > 10$  (dotted orange line), (iii) the same as (i) except Step 5 uses  $T$  samples randomly selected from  $\Theta_s$  to update  $\phi_{\text{mix}}$ , rather than all the available samples (dashed purple line), and (iv) the same as (iii) except that Step 5 is skipped for  $s > 10$  (solid green line). See Table 1 for a summary of these four versions of Algorithm 3. The log Wasserstein distances were computed using the R package ‘transport’. Figure 3 shows that all four procedures perform similarly as the stage number  $s$  increases.

#### 2.4. An Unbiased Warp-U Estimator

Given MCMC samples from  $\pi$ , we are often interested in obtaining an estimate of  $\mathbb{E}_\pi h(\theta)$  for some function  $h(\cdot)$ , where the expectation is taken with respect to  $\theta \in \pi(\theta)$ . Jacob et al. (2020) described a general strategy for *unbiased* estimation of  $\mathbb{E}_\pi h(\theta)$  that involves running two coupled Markov chains  $(\theta_{1,t}, \theta_{2,t-1})$ . Marginally, each chain  $(\{\theta_{1,t}\}_{t=0}^\infty$  or  $\{\theta_{2,t}\}_{t=0}^\infty)$  is updated by the same transition kernel which admits  $\pi$  as its stationary distribution. In addition, the coupled chains should meet the following three requirements:

- R1. As  $t \rightarrow \infty$ ,  $\mathbb{E}[h(\theta_{1,t})] \rightarrow \mathbb{E}_\pi[h(\theta)]$ . There exists an  $\eta > 0$  and  $D < \infty$  such that  $\mathbb{E}[|h(\theta_{1,t})|^{2+\eta}] \leq D$  for all  $t \geq 0$ .
- R2. The meeting time of the two chains  $\tau := \inf\{t \geq 1 : \theta_{1,t} = \theta_{2,t-1}\}$  satisfies  $\mathbb{P}(\tau > t) \leq C\delta^t$  for all  $t \geq 0$ , for some constants  $C < \infty$  and  $\delta \in (0, 1)$ .
- R3. The two chains stay together after meeting, i.e.  $\theta_{1,t} = \theta_{2,t-1}$  for all  $t \geq \tau$ .

Given two coupled chains  $(\theta_{1,t}, \theta_{2,t-1})$  satisfying R1–R3, the unbiased estimation strategy of Jacob et al. (2020) is based on the following relation for a fixed integer  $l$ :

$$\mathbb{E}_\pi[h(\theta)] = \mathbb{E}[h(\theta_{1,l})] + \sum_{t=l+1}^{\infty} \{\mathbb{E}[h(\theta_{1,t})] - \mathbb{E}[h(\theta_{1,t-1})]\}$$

$$\begin{aligned}
&= \mathbb{E}[h(\boldsymbol{\theta}_{1,l})] + \sum_{t=l+1}^{\infty} \{ \mathbb{E}[h(\boldsymbol{\theta}_{1,t})] - \mathbb{E}[h(\boldsymbol{\theta}_{2,t-1})] \} \\
&= \mathbb{E} \left[ h(\boldsymbol{\theta}_{1,l}) + \sum_{t=l+1}^{\tau-1} (h(\boldsymbol{\theta}_{1,t}) - h(\boldsymbol{\theta}_{2,t-1})) \right].
\end{aligned} \tag{15}$$

An unbiased estimator of  $\mathbb{E}_{\pi}[h(\boldsymbol{\theta})]$  based on the coupled chains  $(\boldsymbol{\theta}_{1,t}, \boldsymbol{\theta}_{2,t-1})$  is

$$H_j(\boldsymbol{\theta}_{1,\cdot}, \boldsymbol{\theta}_{2,\cdot}) = h(\boldsymbol{\theta}_{1,j}) + \sum_{t=j+1}^{\tau-1} [h(\boldsymbol{\theta}_{1,t}) - h(\boldsymbol{\theta}_{2,t-1})]. \tag{16}$$

In the above, the last summation term serves as a bias correct and it is zero when  $\tau \leq j + 1$ ; and  $j$  is an arbitrary fixed value. With a single run of the coupled chains, we can obtain an average estimator (averaged across  $j$ ):

$$H_{l:m}(\boldsymbol{\theta}_{1,\cdot}, \boldsymbol{\theta}_{2,\cdot}) = \frac{1}{m-l+1} \sum_{j=l}^m H_j(\boldsymbol{\theta}_{1,\cdot}, \boldsymbol{\theta}_{2,\cdot}) \tag{17}$$

as the final estimator for  $\mathbb{E}_{\pi}h(\boldsymbol{\theta})$ , for some fixed integers  $l$  and  $m$  with  $(l \leq m)$ .

To facilitate the estimation of  $\mathbb{E}_{\pi}h(\boldsymbol{\theta})$  when  $\pi$  is multi-modal, we adapt the strategy of Jacob et al. (2020) to the basic Warp-U sampler in Algorithm 2. This unbiased Warp-U estimation method is detailed in Algorithm 4. We initialise two chains via an initial distribution  $\boldsymbol{\theta}_{1,0}, \boldsymbol{\theta}_{2,0} \sim \pi_0$  (Line 1, Algorithm 4). A one-step update is then conducted for the first chain  $\boldsymbol{\theta}_{1,0}$  (Lines 2–4), which is essentially a single iteration of Algorithm 2. Subsequently, we update the two chains  $(\boldsymbol{\theta}_{1,t}, \boldsymbol{\theta}_{2,t-1})$  jointly (Lines 5–9). Specifically, a Metropolis-Hasting step with maximal coupling or reflection coupling (Jacob et al., 2020) is executed (Line 6), followed by the coupled Warp-U transformation (Line 7) and its inverse (Line 8). The coupled Warp-U transformation strategy is based on the optimal transport coupling (see Supplementary Material, Section S.2.2). This strategy preserves the correct marginal distributions while encouraging proximity of the two chains during their transitions between modes. Note this strategy minimizes the expected squared distance between the two chains after transition, as in Papp and Sherlock (2022).

Full algorithmic details are available in the online Supplementary Material (Section S.2). The requirements R1–R3 are also verified for the proposed algorithm in Section S.2.2. Meanwhile, a Rao-Blackwellization technique is developed in Section S.2.3 to reduce the variance of (16) for estimating  $\mathbb{E}_{\pi}h(\boldsymbol{\theta})$ . Specifically, the summands in (16) are replaced by conditional expectations, where the conditioning is on one or more of the intermediate samples  $\boldsymbol{\theta}_1^{\text{MH}}, \boldsymbol{\theta}_2^{\text{MH}}, \boldsymbol{\theta}_1^*$  and  $\boldsymbol{\theta}_2^*$  in Algorithm 4. Lastly, note that the optimal transport couplings for the Warp-U transformation (Line 7) and its inverse (Line 8) are calculated in two separate steps in Algorithm 4. By integrating Lines 7–8 into a one-step coupling, we can reduce chain meeting time  $\tau$  but with higher computational cost. This version of the algorithm is detailed in Algorithm S.3 in Section S.2.4.

## 2.5. Stochastic Warp-U Bridge Estimation

Having obtained samples from  $\pi$  using the Warp-U sampler in Section 2.3, we may want to use them to estimate the normalising constant  $c$  of  $\pi = q/c$ , which is a special case of the problem of estimating  $\mathbb{E}_{\pi}h(\boldsymbol{\theta})$ . We propose a new estimation strategy which adapts and improves the Warp-U bridge estimator proposed by Wang et al. (2022). The main limitation of the Warp-U bridge sampling estimator is that it has high computational cost if  $q$  is expensive to evaluate, which is an important case because many estimation approaches can work well if  $q$  is inexpensive to evaluate (indeed, exact integration can be performed in the limit where evaluating  $q$  is free). The high computational cost of the Warp-U bridge estimator is due to the fact that each evaluation of  $\tilde{q}$  in (8) requires  $K$  evaluations of  $q$ . Overall Algorithm 1 requires  $K(n_1 + n_2)$  evaluations of  $q$  to obtain an estimate  $\hat{c}$ . Thus, although the Warp-U bridge estimator is statistically more efficient than the standard bridge sampling applied to  $\pi$  and  $\phi_{\text{mix}}$ , it is approximately  $K$  times more expensive. Consequently, Wang et al. (2022) found that, given fixed computational resources, Warp-U bridge sampling is only comparable to standard bridge sampling (and is sometimes slightly worse).

**Algorithm 5** Stochastic Warp-U Bridge Sampling

---

**Input:** parameters  $K$  and  $w_k, \mathcal{S}_k, \boldsymbol{\mu}_k$ , for  $k = 1, \dots, K$ , see (6).

- 1: Sample  $\boldsymbol{\theta}_{1,1}, \dots, \boldsymbol{\theta}_{1,n_1} \sim \pi$ .
- 2: **for**  $i = 1, \dots, n_1$  **do**
- 3: (i) sample  $\psi_i$  from the probability  $\varpi(\psi|\boldsymbol{\theta})$  in (7).
- 4: (ii) Set  $\boldsymbol{\theta}_{1,i}^* = \mathcal{F}_{\psi_i}(\boldsymbol{\theta}_{1,i}) = \mathcal{S}_{\psi_i}^{-1}(\boldsymbol{\theta}_{1,i} - \boldsymbol{\mu}_{\psi_i})$ .
- 5: **end for**
- 6: **for** each component  $k$  from 1 to  $K$  **do**
- 7: (A) Sample  $\boldsymbol{\theta}_{2,k,1}, \dots, \boldsymbol{\theta}_{2,k,n_2} \sim N(0, 1)$ ;
- 8: (B) Apply all  $\boldsymbol{\theta}_{1,i}^*$  with  $\psi_i = k$  and the  $n_2$  samples from (A) to compute (20) (for whatever chosen  $\alpha$ )
- 9: **end for**
- 10: Calculate the final estimator  $\hat{c} = \sum_{k=1}^K w_k \hat{c}_k$ .

---

To obtain a more computationally efficient way of estimating  $c$ , we first note that because  $\tilde{q}$  in (8) preserves the normalising constant  $c$ , it implies that  $c = \sum_{k=1}^K w_k c_k$ , where  $c_k$  is the normalising constant of

$$\tilde{q}_k(\boldsymbol{\theta}^*) = \phi(\boldsymbol{\theta}^*) \frac{q(\mathcal{S}_k \boldsymbol{\theta}^* + \boldsymbol{\mu}_k)}{\phi_{\text{mix}}(\mathcal{S}_k \boldsymbol{\theta}^* + \boldsymbol{\mu}_k)}. \quad (18)$$

By the construction of  $\boldsymbol{\theta}^* = \mathcal{F}_\psi(\boldsymbol{\theta})$  and by (8),  $\tilde{q}_k(\boldsymbol{\theta}^*)/c_k = p(\boldsymbol{\theta}^*|\psi = k)$ . In other words, the normalised counterpart of (8) is a mixture density with the form

$$\tilde{\pi}(\boldsymbol{\theta}^*) = \frac{\tilde{q}(\boldsymbol{\theta}^*)}{c} = \sum_{k=1}^K \frac{w_k c_k}{c} \frac{\tilde{q}_k(\boldsymbol{\theta}^*)}{c_k} = \sum_{k=1}^K \tilde{w}_k \tilde{p}_k(\boldsymbol{\theta}^*), \quad (19)$$

where  $\tilde{w}_k = w_k c_k / c$  is the mixture weight for  $\tilde{p}_k(\boldsymbol{\theta}^*) \equiv p(\boldsymbol{\theta}^*|\psi = k)$ , for  $k = 1, \dots, K$ . This immediately suggests that we can apply bridge sampling to estimate each  $c_k$  separately, using the draws  $\mathcal{F}_\psi(\boldsymbol{\theta})$  where  $\psi = k$ , and pairing them with draws from the common auxiliary density  $\phi$ , for all  $k = 1, \dots, K$ .

Our proposed bridge estimation procedure is detailed in Algorithm 5. The algorithm computes  $c_k$  from the  $\phi$  samples  $\boldsymbol{\theta}_{2,k,j}$  and the  $\pi$  samples  $\boldsymbol{\theta}_{1,j}^*$  for which  $\psi_j = k$ , i.e.,

$$\hat{c}_k = \frac{n_2^{-1} \sum_{j=1}^{n_2} \tilde{q}_k(\boldsymbol{\theta}_{2,k,j}) \alpha(\boldsymbol{\theta}_{2,k,j})}{n_1^{-1} \sum_{j \in \mathcal{J}_k} \phi(\boldsymbol{\theta}_{1,j}^*) \alpha(\boldsymbol{\theta}_{1,j}^*)} \quad (20)$$

where  $\mathcal{J}_k = \{j : \psi_j = k\}$  and  $n_{1k} = |\mathcal{J}_k|$  is the cardinality of the index set  $\mathcal{J}_k$ . To estimate  $c$ , we use the weighted sum  $\hat{c}_{\text{SWB}} := \sum_{k=1}^K w_k \hat{c}_k$ . We call our estimator  $\hat{c}_{\text{SWB}}$  the *stochastic* Warp-U bridge (SWB) estimator because it can be viewed as an estimator of the mean normalising constant of a random unnormalised density. Algorithm 5 requires a total of  $n_1 + Kn_2$  evaluations of  $q$ , which is  $(K-1)n_1$  fewer than that needed for Warp-U bridge estimation. In Section 3.2, we prove that, under some conditions,  $\hat{c}_{\text{SWB}}$  is more efficient than Warp-U bridge estimation in terms of asymptotic variance and precision per CPU second. The stochastic Warp-U bridge estimator can in principle be combined with the unbiased estimation method described in Section 2.4, which is a topic for future work and is briefly discussed in Section 6.2.

### 3. Theoretical Justification

#### 3.1. Ergodicity Property

In this subsection, we establish that Algorithm 3 produces an ergodic Markov chain with stationary distribution  $\pi$ . The technical proofs of the theoretical results in this subsection can be found in the online Supplementary Material, Section S.3.

We make use of Condition 1 below, which has previously been employed by Jarner and Hansen (2000) and Atchadé (2006) to ensure the ergodicity of the random walk Metropolis-Hastings algorithm. Let  $\boldsymbol{n}(\boldsymbol{\theta}) = \boldsymbol{\theta}/\|\boldsymbol{\theta}\|_2$  be a unit vector and  $\boldsymbol{m}(\boldsymbol{\theta}) = \nabla\pi(\boldsymbol{\theta})/\|\nabla\pi(\boldsymbol{\theta})\|_2$  be the normalised gradient of  $\pi$ .

**Condition 1** *The density  $\pi$  is super-exponential, i.e.*

$$\limsup_{\|\boldsymbol{\theta}\|_2 \rightarrow \infty} \langle n(\boldsymbol{\theta}), \nabla \log \pi(\boldsymbol{\theta}) \rangle = -\infty,$$

where  $\langle \cdot, \cdot \rangle$  is vector inner product. In addition,  $\pi$  has a regular manifold contour, i.e.,  $\limsup_{\|\boldsymbol{\theta}\|_2 \rightarrow \infty} \langle n(\boldsymbol{\theta}), m(\boldsymbol{\theta}) \rangle < 0$ .

A Gaussian density or a mixture of Gaussian densities is super-exponential. In fact, densities of the form  $\pi(\boldsymbol{\theta}) = h(\boldsymbol{\theta}) \exp(-g(\boldsymbol{\theta}))$  belong to the super-exponential family for many choices of the polynomials  $h(\boldsymbol{\theta})$  and  $g(\boldsymbol{\theta})$  (see Jarner and Hansen, 2000).

Recall that Algorithm 3 contains Algorithm 2 within a for loop. Let  $P_\gamma$  be the transition kernel for Lines 2–6 of Algorithm 2, where  $\gamma$  represents the adaptive parameters of  $\phi_{\text{mix}}$ . Specifically,  $\gamma = \{K, (\boldsymbol{\mu}_k, \mathcal{S}_k, w_k)_{k=1}^K\}$  includes the number of mixture components  $K$ , as well as the weight  $w_k$ , the mean vector  $\boldsymbol{\mu}_k$  and the scale matrix  $\mathcal{S}_k$  of each component. The adaptive nature of Algorithm 3 means that  $\gamma$  has a chance to be updated periodically, but with decreasing probability. We require each  $\gamma$  to belong to a constraint set  $\Gamma$ , which is specified in Condition 2 below.

**Condition 2** *The adaptive parameter  $\gamma = \{K, (\boldsymbol{\mu}_k, \mathcal{S}_k, w_k)_{k=1}^K\}$  always lies inside the set  $\Gamma$  satisfying*

$$0 < K < K_{\max}, w_k \geq 0, \sum_{k=1}^K w_k = 1, \Lambda_{\min} \leq |\mathcal{S}_k| \leq \Lambda_{\max}, \text{ and } \|\boldsymbol{\mu}_k\|_2 \leq C_\mu.$$

*In the above,  $K_{\max} > 1$ ,  $\Lambda_{\max} > \Lambda_{\min} > 0$ , and  $C_\mu > 0$  are constants which may depend on the underlying data (but not the Monte Carlo samples).*

Condition 2 states that the determinants of the scale matrices  $\mathcal{S}_k$  should be bounded from above and below. In numerical implementation, this requirement can be easily satisfied via monitoring the update of  $\phi_{\text{mix}}$ ; components can be split or merged when  $|\mathcal{S}_k|$  gets too large or too small. Condition 2 also requires that the maximum number of mixture components is bounded from above. In applications, it suffices to set  $K_{\max}, C_\mu$  to be some large numbers such that  $\phi_{\text{mix}}$  can reasonably approximate  $\pi$ .

Based on the above conditions, we now establish the ergodicity of Algorithm 3 through three lemmas. Lemma 1 formalises the argument in Section 2.2 that the target density  $\pi$  is the stationary distribution of Algorithm 2.

**Lemma 1** *For each  $\gamma \in \Gamma$ , the transition kernel  $P_\gamma$  for Lines 2–6 of Algorithm 2 satisfies*

$$\int \pi(\boldsymbol{\theta}) P_\gamma(\boldsymbol{\theta}' | \boldsymbol{\theta}) \mu(d\boldsymbol{\theta}) = \pi(\boldsymbol{\theta}'). \quad (21)$$

To further prove that  $\pi$  is also the stationary distribution of Algorithm 3, we need to establish that Algorithm 3 is ergodic, despite its adaptive nature. To achieve this we apply the framework proposed by Roberts and Rosenthal (2007). We will show that the diminishing adaptation and simultaneous strongly aperiodic geometric ergodicity (SSAGE) conditions hold. The diminishing adaptation condition is stated in Lemma 2 below and is straightforward to verify. Indeed, Step 5 of Algorithm 3 automatically guarantees the kernel update happens with probability decreasing to zero.

**Lemma 2** *The sequence of the transition kernels within Algorithm 3 satisfies the diminishing adaptation condition, i.e.,*

$$\lim_{s \rightarrow \infty} \mathbb{P} \left( \sup_{\boldsymbol{\theta} \in \Theta} \|P_{\hat{\gamma}^s}(\cdot | \boldsymbol{\theta}) - P_{\hat{\gamma}^{s+1}}(\cdot | \boldsymbol{\theta})\|_{TV} \geq \delta_1 \right) = 0 \quad (22)$$

for any  $\delta_1 > 0$ , where  $TV$  indicates the total variation distance, and  $\hat{\gamma}^s, \hat{\gamma}^{s+1}$  are the estimated parameters of  $\phi_{\text{mix}}$  used at stage  $s$  and  $s + 1$ , respectively.

Following Roberts and Rosenthal (2007), the family of transition kernels  $\{P_\gamma\}_{\gamma \in \Gamma}$  satisfies the simultaneous strongly aperiodic geometric ergodicity (SSAGE) condition, if the following two properties are satisfied:

- P1. (Minorization) There exists a probability measure  $\omega$ , a compact Borel set  $C \subset \Theta$ , and a constant  $\delta \in (0, 1]$ , such that  $\omega(C) > 0$  and

$$\inf_{\gamma \in \Gamma} P_\gamma(A | \boldsymbol{\theta}) \geq \delta \cdot \omega(A) \cdot I_C(\boldsymbol{\theta}) \quad (23)$$

for any Borel set  $A \subset \Theta$  and any  $\boldsymbol{\theta} \in \Theta$ , where  $I_C$  is the indicator function of  $C$ .

- P2. (Simultaneous Drift) There exists  $b < \infty$ ,  $\lambda \in (0, 1)$ , and a function  $V$  (with  $V(\boldsymbol{\theta}) \geq 1$  and  $\sup_{\boldsymbol{\theta} \in C} V(\boldsymbol{\theta}) < \infty$ ), such that for any  $\boldsymbol{\theta} \in \Theta$  it holds that

$$\sup_{\gamma \in \Gamma} \int V(\boldsymbol{\theta}') P_\gamma(d\boldsymbol{\theta}' | \boldsymbol{\theta}) \leq \lambda V(\boldsymbol{\theta}) + b I_C(\boldsymbol{\theta}). \quad (24)$$

In the literature, the drift function  $V$  is usually taken as  $V(\boldsymbol{\theta}) = c_\alpha \pi^{-\alpha}(\boldsymbol{\theta})$  for some constant  $c_\alpha$  and  $\alpha \in (0, 1)$ . The SSAGE condition implies that the family of transition kernels  $\{P_\gamma\}_{\gamma \in \Gamma}$  is uniformly geometrically ergodic. Hence the  $m$  step transition kernel  $P_\gamma^m$  of Algorithm 2 has the property that  $\sup_{\gamma \in \Gamma} \|P_\gamma^m(\boldsymbol{\theta}, \cdot) - \pi(\cdot)\|_{TV} \leq R\rho^m V(\boldsymbol{\theta})$ , for some  $\rho < 1$  and  $R < \infty$  (e.g., see equation (2.14) of Atchadé, 2006).

The geometric drift property (P2) requires an additional restriction on  $\Gamma$  which regulates the behaviour of the Warp-U transformation of  $\boldsymbol{\theta}$  when  $\|\boldsymbol{\theta}\|_2 \rightarrow \infty$ . Specifically, when  $\|\boldsymbol{\theta}\|_2 \rightarrow \infty$ , we impose an upper bound on

$$U(\boldsymbol{\theta}) := \mathbb{E}V(\mathcal{G}_{\psi', \psi}(\boldsymbol{\theta})) / V(\boldsymbol{\theta}) = \sum_{\psi, \psi'=1}^K [V(\mathcal{G}_{\psi', \psi}(\boldsymbol{\theta})) / V(\boldsymbol{\theta})] \times p(\psi', \psi | \boldsymbol{\theta}), \quad (25)$$

where the above expectation is taken with respect to the random transformation  $\mathcal{G}_{\psi', \psi}$ , and  $p(\psi', \psi | \boldsymbol{\theta})$  is defined in (11). Let  $Q(\boldsymbol{\theta}, \cdot)$  denote the measure of  $\mathcal{N}(\boldsymbol{\theta}, \sigma^2 \mathbf{I})$  which corresponds to the MH proposal in Step (i) of Algorithm 2, and  $p(\cdot | \boldsymbol{\theta})$  denote the density function of this proposal. Meanwhile, let  $\mathcal{R}(\boldsymbol{\theta})$  be set of  $\boldsymbol{\theta}'$  with acceptance probability less than 1 when starting from  $\boldsymbol{\theta}$ , i.e.,

$$\mathcal{R}(\boldsymbol{\theta}) = \{\boldsymbol{\theta}' \in \Theta : \pi(\boldsymbol{\theta}') p(\boldsymbol{\theta} | \boldsymbol{\theta}') < \pi(\boldsymbol{\theta}) p(\boldsymbol{\theta}' | \boldsymbol{\theta})\}.$$

Lastly, let  $\overline{Q} := \limsup_{\|\boldsymbol{\theta}\|_2 \rightarrow \infty} Q(\boldsymbol{\theta}, \mathcal{R}(\boldsymbol{\theta}))$ . We use the following technical restriction on  $\Gamma$ .

**Condition 3** *The adaptive parameter set  $\Gamma$  satisfies*

$$\limsup_{\|\boldsymbol{\theta}\|_2 \rightarrow \infty} \sup_{\gamma \in \Gamma} U(\boldsymbol{\theta}) < 1 / \overline{Q}. \quad (26)$$

We emphasise that  $U(\boldsymbol{\theta})$  depends on the adaptive parameter  $\gamma$  through the random transformation  $\mathcal{G}_{\psi', \psi}$ , as seen in (25). Intuitively, Condition 3 asserts that the ratio  $\pi(\boldsymbol{\theta}) / \pi(\mathcal{G}_{\psi', \psi}(\boldsymbol{\theta}))$  is not expected to be too large when  $\boldsymbol{\theta}$  is very far away from the origin. In other words, when  $\boldsymbol{\theta}$  is a substantial distance from the origin, the stochastic transformation  $\mathcal{G}_{\psi', \psi}$  is expected to push  $\boldsymbol{\theta}$  towards the origin, where the target density is higher. This condition can be easily verified in some simple settings. For example, when the parameter space  $\Theta = \mathbb{R}$  is one-dimensional, suppose the mixture components in  $\phi_{\text{mix}}$  have balanced weights, the scaling  $S_k$ 's are equal (i.e.,  $S_k = S_{k'}$  for  $k \neq k'$ ), and the component means are not arbitrarily close to each other (i.e.,  $|\mu_k - \mu_{k'}| \geq c_\mu$  for all  $k \neq k'$  and for an arbitrarily small constant  $c_\mu > 0$ ). In this case, we can easily see when  $\theta$  is far away from 0, it is almost surely probable that the stochastic transformation either keeps  $\theta$  at its current position or pushes it towards 0. However, in general situations, the technical Condition 3 may not be straightforward to check.

**Remark** *Condition 3 is only technical and regulates the stochastic transformations when  $\boldsymbol{\theta}$  is extremely far away from the origin. This condition can be completely removed by slightly modifying Algorithm 2 in the*

**Table 2.** Number of evaluations of the unnormalised target density  $q$  for different sampling and estimation methods needed to obtain  $n_1$  target draws and  $n_2$  auxiliary draws which are then used in the estimation step. No. Iters represents the number of iterations (accept and reject),  $n_1$  and  $\bar{n}_1$  denote the number of samples and average number of samples at each stage, respectively,  $M$  is the number of stages,  $M_l$  is the number of temperature levels in Parallel Tempering, and  $n_2$  is the number of samples from the auxiliary distribution.

Sampling	No. Iters	Sampling Evals.	Estimation Evals.		
			Bridge	Warp-U	S. Warp-U
Warp-U MCMC	$n_1 M$	$(K + 1)n_1 M$	$n_2$	$Kn_2$	$Kn_2$
Generalised Wang-Landau	$\bar{n}_1 M$	$\bar{n}_1 M$	$n_2$	$(K - 1)n_1 + Kn_2$	$Kn_2$
Parallel Tempering	$2n_1 M_l$	$n_1 M_l$	$n_2$	$(K - 1)n_1 + Kn_2$	$Kn_2$
Unknown Sampling	–	–	$n_1 + n_2$	$Kn_1 + Kn_2$	$n_1 + Kn_2$

following way. Given a pre-specified and arbitrarily large value  $C_\theta > 0$ , we executed Steps (ii)–(v) only when  $\|\boldsymbol{\theta}^{MH}\|_2 \leq C_\theta$ ; otherwise, we set  $\boldsymbol{\theta}_t = \boldsymbol{\theta}^{MH}$ . Correspondingly, the index probability mass function (10) also needs to be changed to

$$\nu(\psi' | \boldsymbol{\theta}^*) \propto \varpi(\psi' | \mathcal{H}_{\psi'}(\boldsymbol{\theta}^*)) \pi(\mathcal{H}_{\psi'}(\boldsymbol{\theta}^*)) |\mathcal{H}'_{\psi'}(\boldsymbol{\theta}^*)| \cdot I(\|\mathcal{H}_{\psi'}(\boldsymbol{\theta}^*)\|_2 \leq C_\theta).$$

See Section S.4 of the online Supplementary Material for more discussions.

**Lemma 3** Under Condition 1–3, the family of transition kernels  $\{P_\gamma\}_{\gamma \in \Gamma}$  for Algorithm 2 satisfies the SSAGE condition.

Finally, Theorem 2 establishes that Algorithm 3 is ergodic. Specifically, the total variation distance between  $\pi$  and the  $s$ -step transition kernel of Algorithm 3 converges to zero as  $s \rightarrow \infty$ .

**Theorem 2** Under Conditions 1–3, the adaptive Warp-U MCMC sampling algorithm (Algorithm 3) produces a Markov chain which is ergodic with the target distribution  $\pi$  as its stationary distribution.

### 3.2. Computational and Statistical Efficiency of Stochastic Bridge Estimation

In this subsection, we demonstrate that, under some conditions, our stochastic bridge estimator has lower asymptotic variance and greater Precision per Second (PpS) than Warp-U bridge estimation. The technical proofs for the theoretical results in this subsection can be found in the online Supplementary Material, Section S.5.

We define PpS as  $1/(\text{RMSE} \times \text{CPU seconds})$ , and assume that other computational costs are negligible compared with evaluating  $q = c\pi$ . Therefore CPU seconds are given by  $C \cdot E \cdot g(q)$ , where  $C$  is a constant,  $g(q)$  is the time taken to evaluate  $q$  once, and  $E$  is the number of evaluations of  $q$  used by the method under consideration. The values of  $E$  for the different methods we compare are shown in the right three columns of Table 2, where  $n_1$  and  $n_2$  denote the number of the samples from the target and auxiliary distribution, respectively. The auxiliary distribution is the standard Gaussian  $\phi$  for Warp-U bridge estimation and stochastic bridge estimation, and  $\phi_{\text{mix}}$  for classical bridge sampling. The number of Warp-U bridge estimation target evaluations is lower in the case of Warp-U MCMC sampling because some of the necessary evaluations have already been computed during the sampling stage.

Under the i.i.d. sample assumption, Meng and Wong (1996) showed that the asymptotic variance of the logarithm  $\hat{\lambda} = \log(\hat{r})$  of the classical bridge estimator (3) is

$$\left(n_1^{-1} + n_2^{-1}\right) \left[(1 - H_A(p_1, p_2))^{-1} - 1\right] + o\left((n_1 + n_2)^{-1}\right), \quad (27)$$

where  $H_A(p_1, p_2)$  is the sample-size adjusted harmonic divergence (5). We consider the setting when  $p_2 = \phi$  (with  $c_2 = 1$ ) and  $p_1$  corresponds to the Warp-U transformed density (19) for comparing the Warp-U bridge estimator ( $\hat{\lambda}_{\text{WB}} = \log(\hat{c}_{\text{WB}})$ ) and the stochastic Warp-U bridge estimator ( $\hat{\lambda}_{\text{SWB}} = \log(\hat{c}_{\text{SWB}})$ ). The

asymptotic variance (27) can not be directly applied to compare  $\hat{\lambda}_{WB}$  and  $\hat{\lambda}_{SWB}$ , because  $H_A$  involves sample sizes and the stochastic Warp-U bridge estimator exploits random subsamples to reduce the computational cost. Theorem 3 below provides an alternative comparison of the asymptotic variance based on the Pearson's  $\chi^2$  divergence,  $\chi_P^2(p_1, p_2) = \int (p_2(\boldsymbol{\theta})/p_1(\boldsymbol{\theta}) - 1)^2 \times p_1(\boldsymbol{\theta})\mu(d\boldsymbol{\theta})$ , which approximates the sample-size adjusted harmonic divergence (5) as  $n_1, n_2 \rightarrow \infty$ , see Nielsen and Nock (2013).

**Theorem 3** *Suppose that the available samples are i.i.d. from  $\pi = q/c$  and the standard Gaussian distribution  $\phi$ . As  $n_1, n_2 \rightarrow \infty$ , suppose that  $n_2/n_1 \rightarrow \beta(> 0)$  and  $\chi_P^2(\phi_{\text{mix}}, \pi) \rightarrow 0$ . Then*

$$\lim_{n_1, n_2 \rightarrow \infty} \frac{(n_1 + n_2)\text{Var}(\hat{\lambda}_{WB})}{\chi_P^2(\phi, \tilde{\pi})} = 1, \quad (28)$$

and

$$\lim_{n_1, n_2 \rightarrow \infty} \frac{(n_1 + n_2)\text{Var}(\hat{\lambda}_{SWB})}{\sum_{k=1}^K \tilde{w}_k^2(1 + \beta)/(\tilde{w}_k + \beta) \cdot \chi_P^2(\phi, \tilde{p}_k)} = 1. \quad (29)$$

The notation  $\tilde{\pi}$ ,  $\tilde{p}_k$  and  $\tilde{w}_k$  is defined in (19).

MCMC draws generally have a complex dependence which is specific to the sampling algorithm used. For simplification, Theorem 3 assumes i.i.d. samples. Theorem 3 also assumes that the sample size ratio  $n_2/n_1$  converges to a constant, and that  $\phi_{\text{mix}}$  approximates  $\pi$  with increasing accuracy as the sample size increases. The result suggests  $\text{Var}(\hat{\lambda}_{SWB})$  can be expected to be smaller than  $\text{Var}(\hat{\lambda}_{WB})$  in certain cases. Consider as an illustrative case the scenario where  $\beta \geq 1$ ,  $K$  is a relatively large, and the mixture components in  $\tilde{\pi}$  have approximately equal weights (i.e.  $\tilde{w}_k \approx 1/K \approx 0$  such that  $\tilde{w}_k + \beta \approx \beta$ ). Then, the denominator in (29) approximately equals

$$\sum_{k=1}^K \tilde{w}_k^2(1 + \beta)/(\tilde{w}_k + \beta) \cdot \chi_P^2(\phi, \tilde{p}_k) \approx (1 + 1/\beta) \times \left[ \frac{1}{K} \sum_{k=1}^K \chi_P^2(\phi, \tilde{p}_k) \right] / K. \quad (30)$$

The quantity inside the square brackets is the average of the component divergences  $\chi_P^2(\phi, \tilde{p}_k)$ , and this is further divided by  $K$  (which is large). Thus, intuitively, we can expect (30) to be smaller than the denominator of (28) in this setting. In the following, we further exploit Lemma 3 to rigorously characterise when  $\text{Var}(\hat{\lambda}_{SWB})$  will be smaller than  $\text{Var}(\hat{\lambda}_{WB})$  asymptotically.

Based on (28) and (29), the Warp-U bridge and stochastic Warp-U bridge estimators have small asymptotic variance when  $\tilde{\pi}$  or  $\tilde{p}_k$ , respectively, is close to  $\phi$ . For our stochastic Warp-U bridge estimator, the ideal case is that each mixture component  $\tilde{p}_k$  perfectly matches the transformation target  $\phi$ . In that ideal case, the estimator would have zero asymptotic variance. In practice, we can not expect such perfect agreement with  $\phi$ . We measure the discrepancy by  $d_k(\boldsymbol{\theta}) = \tilde{p}_k(\boldsymbol{\theta})/\phi(\boldsymbol{\theta}) - 1$ , and collect the weighted discrepancy for all densities  $\tilde{p}_k$  in the mixture (19) as a vector

$$\mathbf{d}(\boldsymbol{\theta}) = (\tilde{w}_1 d_1(\boldsymbol{\theta}), \tilde{w}_2 d_2(\boldsymbol{\theta}), \dots, \tilde{w}_K d_K(\boldsymbol{\theta}))^\top. \quad (31)$$

Note that the sign of  $d_k(\boldsymbol{\theta})$  reflects the transformation bias. When  $d_k(\boldsymbol{\theta}) > 0$ , the transformed density  $\tilde{p}_k$  overestimates  $\phi$  at  $\boldsymbol{\theta}$ , whereas when  $d_k(\boldsymbol{\theta}) < 0$ , it underestimates  $\phi$  at  $\boldsymbol{\theta}$ . The overall bias for the mixture distribution  $\tilde{\pi}$  at  $\boldsymbol{\theta}$  is measured by  $\mathbf{1}^\top \mathbf{d}(\boldsymbol{\theta})$ . Based on this intuition, we decompose the discrepancy vector  $\mathbf{d}(\boldsymbol{\theta})$  as

$$\mathbf{d}(\boldsymbol{\theta}) = \mathbf{P}_1 \mathbf{d}(\boldsymbol{\theta}) + (\mathbf{I} - \mathbf{P}_1) \mathbf{d}(\boldsymbol{\theta}). \quad (32)$$

where  $\mathbf{P}_1 = (1/K)\mathbf{1}\mathbf{1}^\top$  is the orthonormal projection matrix onto  $\text{span}\{\mathbf{1}\}$ . Equation (32) implies that the weighted sum of the component discrepancies  $\chi_P^2(\phi, \tilde{p}_k)$  can be written as

$$\sum_{k=1}^K \tilde{w}_k^2 \chi_P^2(\phi, \tilde{p}_k) = \int \|\mathbf{d}(\boldsymbol{\theta})\|_2^2 \phi(\boldsymbol{\theta}) \mu(d\boldsymbol{\theta})$$



$$= \underbrace{\int \|\mathbf{P}_1 \mathbf{d}(\boldsymbol{\theta})\|_2^2 \phi(\boldsymbol{\theta}) \mu(d\boldsymbol{\theta})}_{\text{(I)}} + \underbrace{\int \|(\mathbf{I} - \mathbf{P}_1) \mathbf{d}(\boldsymbol{\theta})\|_2^2 \phi(\boldsymbol{\theta}) \mu(d\boldsymbol{\theta})}_{\text{(II)}}. \quad (33)$$

In the above, the average magnitude of  $\mathbf{d}(\boldsymbol{\theta})$  across all  $\boldsymbol{\theta}$  is decomposed into two parts: term (I) equals  $\chi_P^2(\phi, \tilde{\pi})/K$  and reflects the bias of  $\tilde{\pi}$  averaged across  $\boldsymbol{\theta}$ ; term (II) measures the magnitude of the remaining discrepancy between the Warp-U transformed components and  $\phi$ . Term (I) may be interpreted as the “systematic bias”. The following theorem reveals that when (I) is a non-negligible source of discrepancy, our stochastic Warp-U bridge estimator will have better performance than the Warp-U bridge estimator (Wang et al., 2022) in terms of asymptotic variance and precision per second.

**Theorem 4** *Suppose that  $\beta \geq 1, K \geq 3$ , and the conditions in Lemma 3 hold. Then, when*

$$\int \|\mathbf{P}_1 \mathbf{d}(\boldsymbol{\theta})\|_2^2 \phi(\boldsymbol{\theta}) \mu(d\boldsymbol{\theta}) \geq \beta_{1K} \int \|(\mathbf{I} - \mathbf{P}_1) \mathbf{d}(\boldsymbol{\theta})\|_2^2 \phi(\boldsymbol{\theta}) \mu(d\boldsymbol{\theta}), \quad (34)$$

with  $\beta_{1K} = (\beta + 1)/(\beta(K - 1) - 1)$ , we have

$$\limsup_{n_1, n_2 \rightarrow \infty} [\text{Var}(\hat{\lambda}_{SWB})/\text{Var}(\hat{\lambda}_{WB})] \leq 1; \quad (35)$$

and

$$\liminf_{n_1, n_2 \rightarrow \infty} [\text{PpS}(\hat{\lambda}_{SWB})/\text{PpS}(\hat{\lambda}_{WB})] \geq \frac{(1 + \beta)K}{1 + \beta K}. \quad (36)$$

When  $\beta \geq 1$ , we have  $\beta_{1K} \leq 3/(K - 1)$  and hence  $\beta_{1K} \|(\mathbf{I} - \mathbf{P}_1) \mathbf{d}(\boldsymbol{\theta})\|_2^2 \leq 3/(K - 1) \|(\mathbf{I} - \mathbf{P}_1) \mathbf{d}(\boldsymbol{\theta})\|_2^2$ . Based on this, a sufficient condition for (34) is that

$$\int \|\mathbf{P}_1 \mathbf{d}(\boldsymbol{\theta})\|_2^2 \phi(\boldsymbol{\theta}) \mu(d\boldsymbol{\theta}) \geq [3/(K - 1)] \times \int \|(\mathbf{I} - \mathbf{P}_1) \mathbf{d}(\boldsymbol{\theta})\|_2^2 \phi(\boldsymbol{\theta}) \mu(d\boldsymbol{\theta}). \quad (37)$$

The right hand side of (37) measures the dimension-adjusted size of  $\mathbf{d}(\boldsymbol{\theta})$  inside  $\text{span}(\mathbf{1})^\perp$  (multiplied by 3), because  $\dim(\text{span}(\mathbf{1})^\perp) = K - 1$ . The sufficient condition (37) means that, adjusted by subspace dimension, the average size of  $\mathbf{d}(\boldsymbol{\theta})$  inside  $\text{span}(\mathbf{1})$  should be three times as large as the average size of  $\mathbf{d}(\boldsymbol{\theta})$  inside  $\text{span}(\mathbf{1})^\perp$ .

In practice, condition (34) will be satisfied if the  $\tilde{p}_k$ 's tend to jointly over-estimate (or under-estimate)  $\phi$  across non-negligible regions of  $\Theta$ . For example, if the target density  $\pi$  is a mixture of  $t$ -distribution while  $\phi_{\text{mix}}$  is a mixture of Gaussians, then each component of  $\phi_{\text{mix}}$  could over-estimate around the modes and under-estimate the tails of each corresponding component of the target distribution. Systematic bias could potentially also arise from bias of the estimation method used for fitting  $\phi_{\text{mix}}$  to  $\pi$ . In all our numerical studies, the stochastic Warp-U bridge estimator performs better than the original Warp-U bridge estimator.

The precision per second comparison (36) takes the number of evaluations of  $q$  into account. Recall that the Warp-U bridge estimator requires  $(n_1 + n_2)K$  evaluations of  $q$ , while the stochastic Warp-U bridge estimator requires  $n_1 + n_2K$  evaluations. As  $n_1 \rightarrow \infty$  and  $n_2/n_1 \rightarrow \beta > 0$ , the ratio  $(n_1 + n_2)K/(n_1 + n_2K)$  converges to  $(1 + \beta)K/(1 + \beta K)$ , which is the right hand side of (36).

## 4. Simulation Studies

We present simulation studies to illustrate the effectiveness of our methodology: Section 4.1 focuses on the Warp-U MCMC sampling method described by Algorithm 3, and Section 4.3 focuses on the stochastic Warp-U bridge estimation method described by Algorithm 5 when combined with various sampling strategies. Our main simulation studies include 4-dimensional, 10-dimensional, and 30-dimensional examples. The empirical performance of unbiased Warp-U estimation (Algorithm 4) is examined in Section 4.4. In Section 4.5, we present some challenges and solutions in the context of the 50-dimensional setting discussed in Wang et al. (2022), which has complex density contours and heavy tails.

#### 4.1. Comparison of Sampling Methods

We now consider a 4-dimensional multivariate Gaussian mixture target distribution  $\pi$  and compare the performance of our Warp-U MCMC sampling method to Parallel Tempering (PT) and the Metropolis-Hastings (MH) algorithm with a fixed proposal distribution. PT (Geyer, 1991) is a widely used method designed to sample from multimodal target distributions, but it is necessary to tune the temperature levels, which can be time-consuming. For tuning the temperature levels, we apply the method of Atchadé et al. (2011) which iteratively selects the inverse temperatures by the stochastic approximation algorithm given in Robbins and Monro (1951) and Andrieu and Robert (2001). For MH, we set the proposal density to be  $\phi_{\text{mix}}$ , i.e., the same density used by our Warp-U MCMC sampler. The unnormalised target distribution is given by

$$\begin{aligned} q(\boldsymbol{\theta}) &= \frac{1}{15} \exp\left(-\frac{1}{2}(\boldsymbol{\theta} + \mathbf{11})^\top (\boldsymbol{\theta} + \mathbf{11})\right) + \frac{2}{15} \exp\left(-\frac{1}{2}(\boldsymbol{\theta} - \mathbf{12})^\top (\boldsymbol{\theta} - \mathbf{12})\right) \\ &+ \frac{3}{15} \exp\left(-\frac{1}{2}(\boldsymbol{\theta} + \mathbf{8})^\top (\boldsymbol{\theta} + \mathbf{8})\right) + \frac{4}{15} \exp\left(-\frac{1}{2}(\boldsymbol{\theta} - \mathbf{7})^\top (\boldsymbol{\theta} - \mathbf{7})\right) \\ &+ \frac{5}{15} \exp\left(-\frac{1}{2}(\boldsymbol{\theta} + \mathbf{2})^\top (\boldsymbol{\theta} + \mathbf{2})\right), \end{aligned}$$

where bold numbers indicate the vectors in  $\mathbb{R}^4$ , e.g.,  $\mathbf{2} = (2, 2, 2, 2)^\top$ . Note that some of the modes (especially  $-\mathbf{2}$  and  $\mathbf{7}$ ) are well separated, and therefore a simple Metropolis-Hastings algorithm with a Gaussian proposal is not expected to work well.

We apply Algorithm 3 with  $T = 4000$  (number of samples at each stage),  $M = 11$  (number of stages), and  $K = 10$  (number of components). We repeat the simulation 50 times, and use kernel density estimation to infer the target density for each simulation, and thereby obtain approximate pointwise 95% confidence intervals. Figure 4 shows the inferred density and pointwise 95% confidence interval (middle dash-dot blue line and blue shaded regions) based on samples obtained at different stages of our Warp-U MCMC sampling algorithm: (i) based on the initial samples (top left panel), (ii) based on samples obtained in stage 1 (top right panel), and (iii) based on stage 7 samples (bottom left panel), respectively. The solid red lines show the true target density. We can see that for the initial samples, the confidence interval is highly inconsistent with the target density (since the initial sampling is from a uniform distribution), but that the confidence interval at stage 7 covers the target density well (88.3% coverage). We found that the square of the inverse of the log Wasserstein distance between the true marginal density and the estimated marginal is well approximated by a linear function of the stage number, see the bottom right of Figure 4.

Figure 5 shows the log Wasserstein distance between the true target density and the density estimated from samples, as a function of target evaluations, when the sampling method is our adaptive Warp-U MCMC method (solid blue lines) or PT (dashed orange lines). Figure 5 shows that the samples obtained via our adaptive Warp-U MCMC sampler better approximate the true target density than those obtained via PT, for a given number of target evaluations. In other words, in this example, our approach has lower computational cost than PT for a given level of accuracy.

Figure 6 shows the trace plot and auto-correlation function (ACF) for our non-adaptive Warp-U MCMC sampler specified in Algorithm 2 (left column) and the Metropolis-Hastings (MH) algorithm with proposal density  $\phi_{\text{mix}}$  (right column). We use the non-adaptive version of our sampler to avoid having to change the proposal density of MH algorithm that we are comparing to at each stage and simplify the comparison. The Gaussian mixture distribution  $\phi_{\text{mix}}$  used for this non-adaptive version is given by (S.4) in Section S.1 of the online Supplementary Material. The trace and ACF plots show that the Warp-U transformation used in Algorithm 2 greatly reduces the dependence between samples compared with the Metropolis-Hastings approach, and facilitates jumps between modes leading to a larger effective sample size for the Warp-U MCMC sampler.

#### 4.2. Comparison of Sampling Methods in High Dimension

A notable limitation of PT is that it converges slowly for high dimensional mixture distributions whose components have unequal variances, as Woodard et al. (2009) demonstrated theoretically. Woodard et al. (2009) provided a theoretical demonstration of PT's slow convergence in certain high-dimensional contexts,

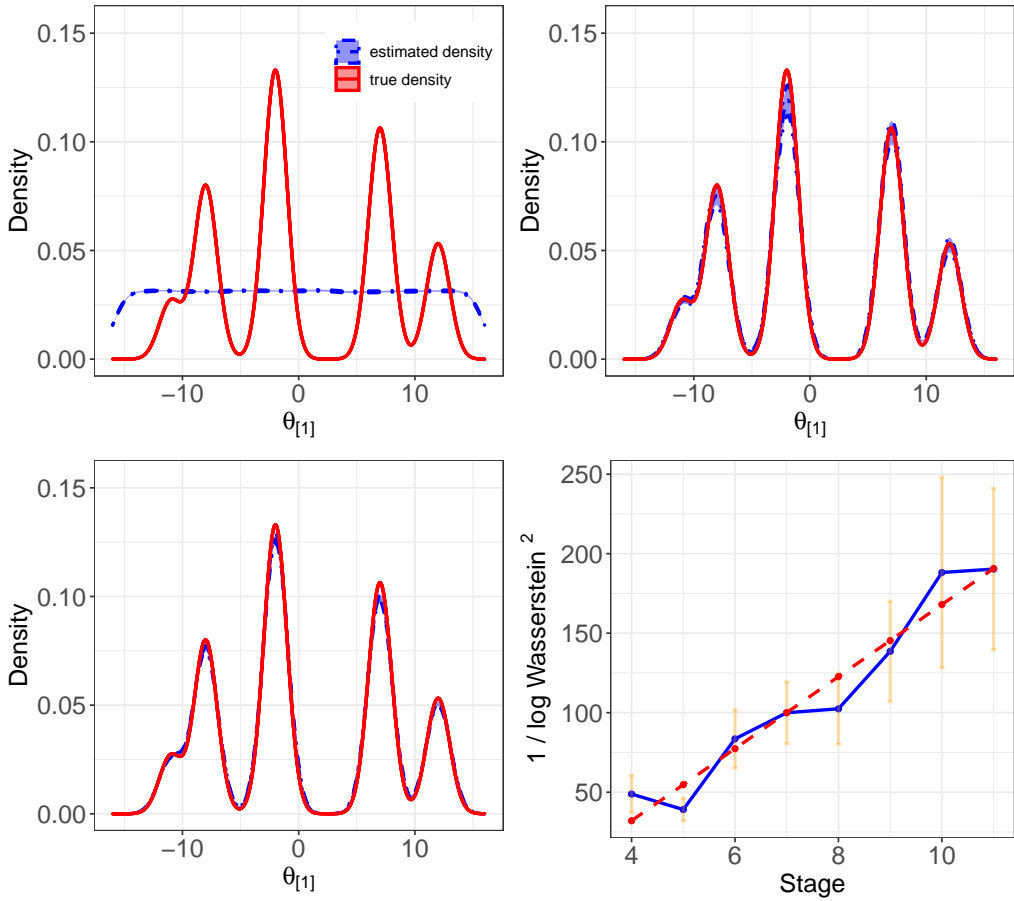


Fig. 4: The top left, top right, and bottom left panels show the true target density (red line) and the density estimated from samples obtained using our adaptive Warp-U MCMC sampler (middle dash-dot blue line) before the first, second, and eighth stage of Algorithm 3, respectively. The blue shaded regions show pointwise 95% confidence intervals (marked by the upper and lower dash-dot blue lines). The bottom right panel shows the square of the 1/log Wasserstein distance (solid blue line) between the true marginal density (the first dimension of the target) and the estimated marginal density at different stages of the algorithm, as well as 95% confidence intervals (solid orange lines) and a linear fit (dashed red line).

especially when the target distribution is a mixture of Gaussians with distinct variances. We examine the performance of PT and Warp-U sampler in two related settings.

In the first setting, we adopt the target distribution in Woodard et al. (2009):

$$q(\boldsymbol{\theta}) = \frac{1}{2\bar{\sigma}_1^d} \exp\left(-\frac{1}{2\bar{\sigma}_1^2}(\boldsymbol{\theta} + \mathbf{1})^\top(\boldsymbol{\theta} + \mathbf{1})\right) + \frac{1}{2\bar{\sigma}_2^d} \exp\left(-\frac{1}{2\bar{\sigma}_2^2}(\boldsymbol{\theta} - \mathbf{1})^\top(\boldsymbol{\theta} - \mathbf{1})\right),$$

and we compare the performance of PT and Warp-U sampler as the dimension  $d$  increases. Specifically, in this experiment, we set  $\bar{\sigma}_1^2 = 0.8$  and  $\bar{\sigma}_2^2 = 0.2$ , and vary the dimension  $d \in \{5, 10, 30, 50, 80, 100, 300, 1000\}$ .

For PT, we run 20 chains with equally spaced inverse temperature. On the other hand, recall the Warp-U sampler in Algorithm 2 requires the specification of the auxiliary density  $\phi_{\text{mix}}$ . The adaptive version in Algorithm 3 is less sensitive to the particular form of  $\phi_{\text{mix}}$ , which is only used for initialisation. However, for simplicity, in this experiment, we test the Warp-U sampler in Algorithm 2 with two choices of  $\phi_{\text{mix}}$  as follows.

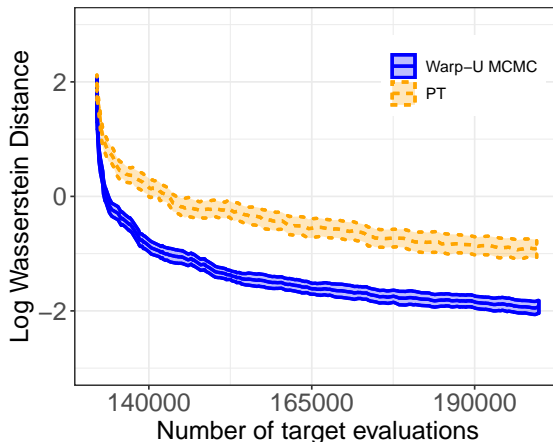


Fig. 5: Log Wasserstein distance between the true target density and estimated density constructed using our adaptive Warp-U MCMC method (centre solid blue line) and PT (centre dashed orange line), as well as pointwise 95% confidence intervals (shaded regions).

Given  $q$ , a simplistic choice of the auxiliary distribution would nbe

$$\phi_{\text{mix},1}(\boldsymbol{\theta}) = \frac{1}{2}\phi(\boldsymbol{\theta} - \boldsymbol{\mu}_1) + \frac{1}{2}\phi(\boldsymbol{\theta} - \boldsymbol{\mu}_2), \quad (38)$$

where  $\boldsymbol{\mu}_1 = -\mathbf{1}$  and  $\boldsymbol{\mu}_2 = \mathbf{1}$ . Here the modes  $(\boldsymbol{\mu}_1, \boldsymbol{\mu}_2)$  can be estimated from random initial points. It is a simplistic choice because it ignores the variances. A more principled choice would attempt to model the unknown variances, such as

$$\phi_{\text{mix},2}(\boldsymbol{\theta}) = \int \frac{1}{2\sigma_1^d} \phi((\boldsymbol{\theta} - \boldsymbol{\mu}_1)/\sigma_1) p(\sigma_1^2) d\sigma_1^2 + \int \frac{1}{2\sigma_2^d} \phi((\boldsymbol{\theta} - \boldsymbol{\mu}_2)/\sigma_2) p(\sigma_2^2) d\sigma_2^2, \quad (39)$$

which enables us to account for some uncertainty regarding the variances. In this experiment, we set  $p(\sigma_1^2)$  and  $p(\sigma_2^2)$  to be the inverse Gamma distribution,  $\text{Inv-Gamma}(a, b)$ , with shape parameter  $a = 2.25$  and scale parameter  $b = 1.25$ . Note, when  $\sigma_1^2 \sim p(\sigma_1^2)$ , we have  $\mathbb{E}(\sigma_1^2) = 1$  and  $\text{Var}(\sigma_1^2) = 4$ . This reflects our weak knowledge of the variances in the target  $q$ . When the Warp-U sampler runs with (39), in addition to the primary mixture component index  $\psi \in \{1, 2\}$ , we also need to sample the variance  $\sigma_\psi^2$ . The implementation details for the Warp-U sampler with (39) are provided in Section S.7.1 of the Online Supplements.

For each specified value of  $d$ , we run each algorithm 20 times to understand their convergence properties. In each run, the initial sample is drawn from the standard Gaussian distribution, and the first 1000 samples are discarded, and the subsequent 4000 samples are retained. The simulation outcomes from one run are depicted in Figure 8. In the figure, each panel shows the density plot for  $(\theta_1, \theta_d)$ , i.e., the joint density plot for the first and the last dimension. Note each 2-dimensional density plot is for MCMC samples. Each panel also shows the marginal histogram for MCMC samples, and the black curves represent the target marginal densities. The three columns are for PT, Warp-U sampler with  $\phi_{\text{mix},1}$  in (38), and Warp-U sampler with  $\phi_{\text{mix},2}$  in (39), respectively. The four rows correspond to dimension  $d = 10, 30, 100$ , and 1000, respectively. When the dimension equals  $d = 10$ , all three algorithms accurately detects two local modes of the target density. When  $d = 30$ , the Warp-U samples depicts the two modes, while PT fails to do so. When  $d \geq 100$ , both PT and the Warp-U sampler with  $\phi_{\text{mix},1}$  fail to discover two local modes, while the samples from Warp-U sampler with  $\phi_{\text{mix},2}$  maintain a good representation of the target.

The left panel of Figure 7 presents the Wasserstein distance between i.i.d samples from the target joint density and the Markov chain samples, for the two dimensions  $(\theta_1, \theta_d)$ . The distance is averaged across

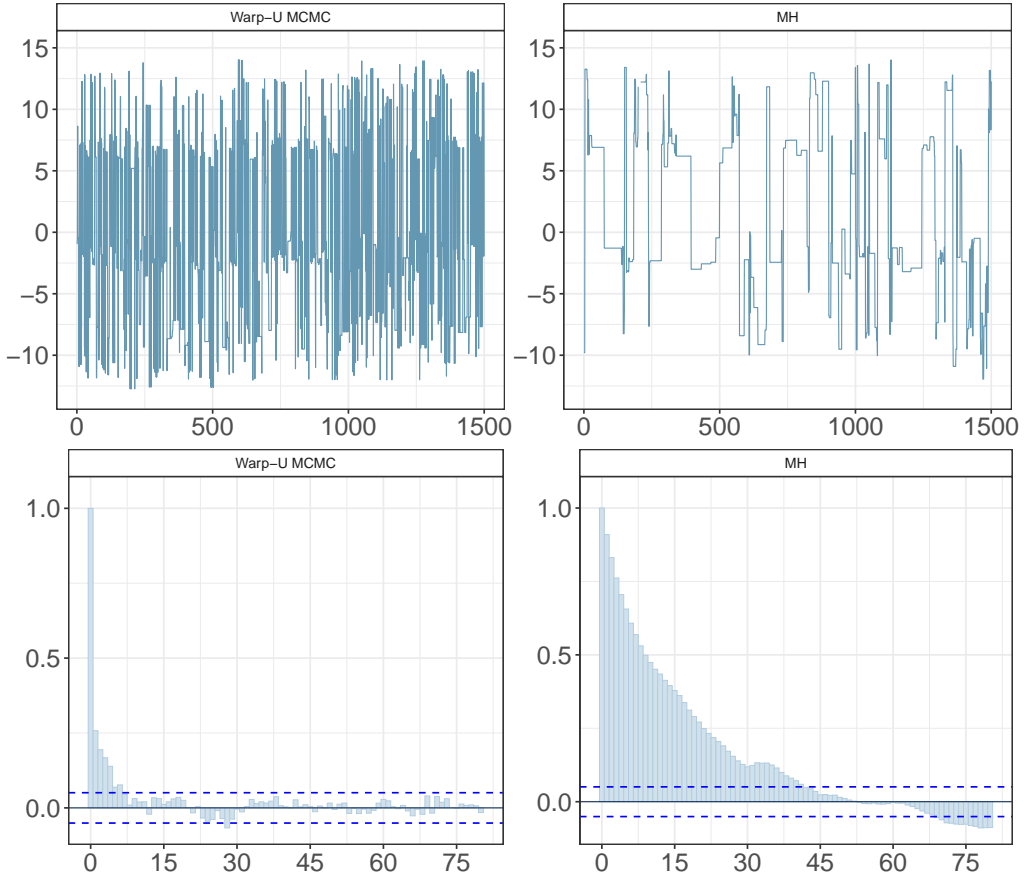


Fig. 6: Trace and autocorrelation plots for our Warp-U MCMC method (left column) and MH with proposal density  $\phi_{\text{mix}}$  (right column). The y-axis of the panels in the first row is the first dimension of the samples from the target density, i.e.,  $\theta_{[1]}$ .

20 replicates. As the dimension  $d$  increases, the Warp-U sampler using (39) consistently achieves better accuracy than PT. While the performance of the Warp-U sampler with (38) does decline as  $d$  increases, it still outperforms PT in moderate dimensions.

We note that the average computing time for each run of PT, Warp-U sampler with  $\phi_{\text{mix},1}$  in (38), and Warp-U sampler with  $\phi_{\text{mix},2}$  are 7.44 min, 0.34 min, 47.68 min, respectively. Warp-U sampler with  $\phi_{\text{mix},2}$  took substantially longer because we need to use metropolis algorithm to draw the inverse Warp-U transformation. But this significantly longer running time is worthwhile in the sense that running the first two algorithms for this long would not get them out of their trapped regions.

In the second simulation setting, we consider the target distribution:

$$q(\theta) = \sum_{k=1}^2 \frac{1}{2|\bar{\mathbf{D}}_k|^{1/2}} \exp\left(-\frac{1}{2}(\theta - \mu_k)^\top \bar{\mathbf{D}}_k^{-1}(\theta - \mu_k)\right). \quad (40)$$

The above is also a Gaussian mixture distribution with two components. The elements of the first mean vector  $\mu_1$  are drawn from  $\text{Uniform}(-2.5, -1.5)$ ; the elements of the second mean vector  $\mu_2$  are drawn from  $\text{Uniform}(1.5, 2.5)$ . Besides, for  $k = 1, 2$ , the covariance matrix  $\bar{\mathbf{D}}_k = \text{diag}(\bar{\mathbf{D}}_{k1}, \bar{\mathbf{D}}_{k2}, \dots, \bar{\mathbf{D}}_{k5}) \in \mathbb{R}^{d \times d}$  is

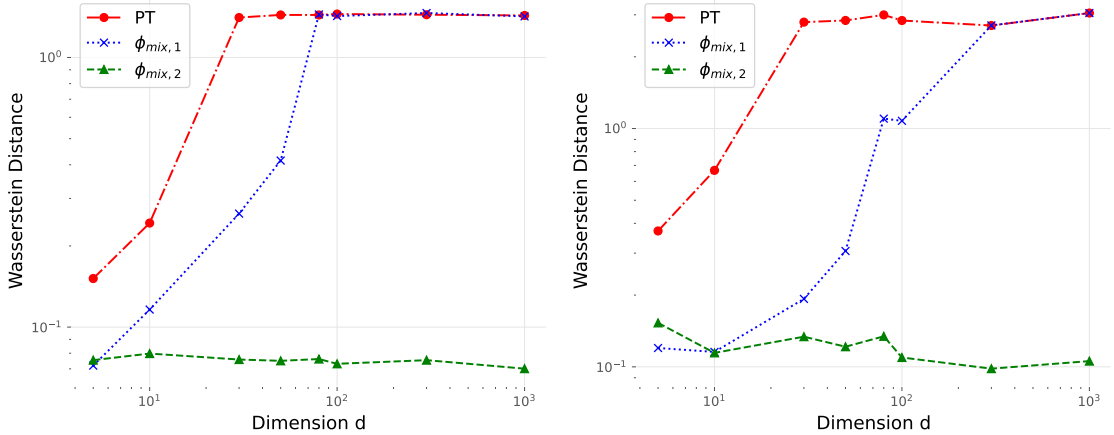


Fig. 7: Comparison of sampling methods in high dimension. The Wasserstein distance between MCMC samples and true target i.i.d samples for Setting 1 (left panel) and Setting 2 (right panel). The distance is computed for the joint marginal  $(\theta_1, \theta_d)$  and is averaged across 20 simulation replicates.

diagonal of size  $d$ . For  $j = 1, \dots, 5$ , the block  $\bar{\mathbf{D}}_{kj} = \text{diag}(\bar{\sigma}_{kj}^2, \bar{\sigma}_{kj}^2, \dots, \bar{\sigma}_{kj}^2) \in \mathbb{R}^{(d/5) \times (d/5)}$  has exactly the same value for its diagonal elements. Specifically, we use

$$\begin{aligned} (\bar{\sigma}_{11}^2, \bar{\sigma}_{12}^2, \bar{\sigma}_{13}^2, \bar{\sigma}_{14}^2, \bar{\sigma}_{15}^2) &= (0.25, 0.3, 0.35, 0.4, 0.45), \text{ and} \\ (\bar{\sigma}_{21}^2, \bar{\sigma}_{22}^2, \bar{\sigma}_{23}^2, \bar{\sigma}_{24}^2, \bar{\sigma}_{25}^2) &= (1, 0.95, 0.9, 0.85, 0.8), \end{aligned}$$

for the two mixture components, respectively.

In this setting, we run Warp-U sampler with the auxiliary distribution:

$$\phi_{\text{mix},1}(\boldsymbol{\theta}) = \frac{1}{2}\phi(\boldsymbol{\theta} - \boldsymbol{\mu}_1) + \frac{1}{2}\phi(\boldsymbol{\theta} - \boldsymbol{\mu}_2), \quad (41)$$

where the mean vectors  $\boldsymbol{\mu}_1, \boldsymbol{\mu}_2$  are the same as in (40). Meanwhile, we will also run Warp-U sampler with another auxiliary distribution:

$$\phi_{\text{mix},2}(\boldsymbol{\theta}) = \sum_{k=1}^2 \int \frac{1}{2|\mathbf{D}_k|^{1/2}} \phi(\mathbf{D}_k^{-1/2}(\boldsymbol{\theta} - \boldsymbol{\mu}_k)) \prod_{j=1}^5 p(\sigma_{kj}^2) d\sigma_{k1}^2 \dots d\sigma_{k5}^2. \quad (42)$$

In the above,  $\mathbf{D}_k = \text{diag}(\mathbf{D}_{k1}, \mathbf{D}_{k2}, \dots, \mathbf{D}_{k5}) \in \mathbb{R}^{d \times d}$  has exactly the same diagonal structure as  $\bar{\mathbf{D}}_k$  in (40), but with unknown values of  $\sigma_{kj}^2$  on the diagonal of  $\mathbf{D}_{kj}$ . Each  $p(\sigma_{kj}^2)$  is an inverse Gamma distribution with with shape parameter  $a = 2.25$  and scale parameter  $b = 1.25$ .

The result for one simulation replicate is shown in Figure 9. The interpretation is similar as that for Figure 8. For PT in the first column, when  $d = 10$ , though it discovers two local modes of the target density, the Markov chain samples under-represent the mode with smaller variances. When  $d \geq 30$ , PT samples only discover the mode with larger variance. For Warp-U sampler with  $\phi_{\text{mix},1}$  in the second column, its samples are no longer an accurate portrayal of the two local modes when  $d \geq 100$ . For Warp-U sampler with  $\phi_{\text{mix},2}$  in the third column, its samples consistently maintain a good representation of the target. In the right panel of Figure 7, we show the Wasserstein distance between the MCMC sampled  $(\theta_1, \theta_d)$  and the i.i.d samples from the target density. The distance is averaged across 20 simulation replicates. Warp-U sampler with  $\phi_{\text{mix},2}$  consistently generates high-quality samples across distinct specifications of the dimension.

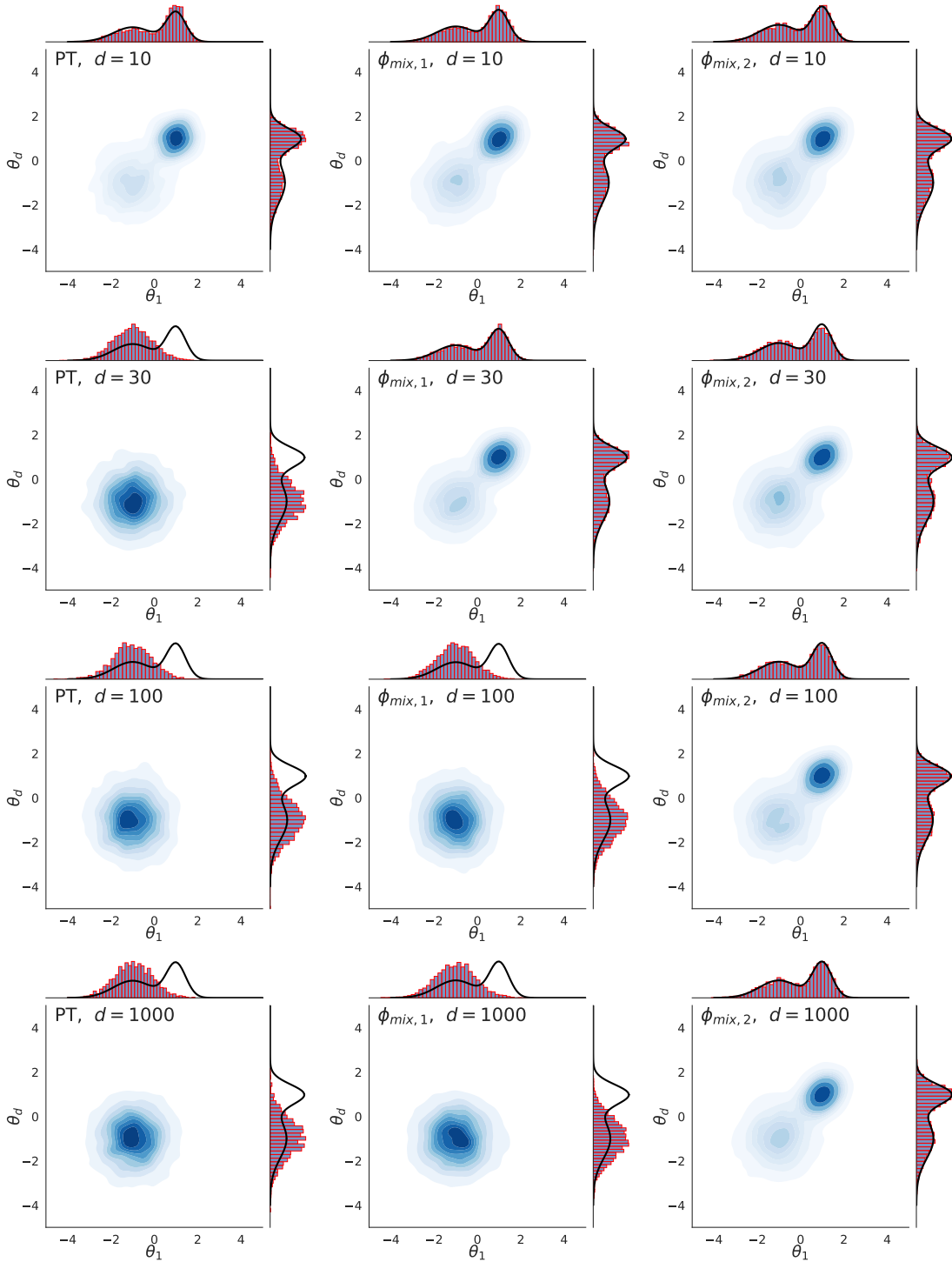


Fig. 8: Comparison of PT and Warp-U sampler in Setting 1. Each panel shows the density plot for  $(\theta_1, \theta_d)$ , which is drawn by one run of a MCMC sampler. Each panel also shows the marginal histogram for the Markov chain samples, and the black curves are the true marginal density. The three columns are for PT, Warp-U sampler with  $\phi_{mix,1}$  (see (38)), and Warp-U sampler with  $\phi_{mix,2}$  (see (39)), respectively. The four rows correspond to dimension  $d = 10, 30, 100, 1000$ , respectively.

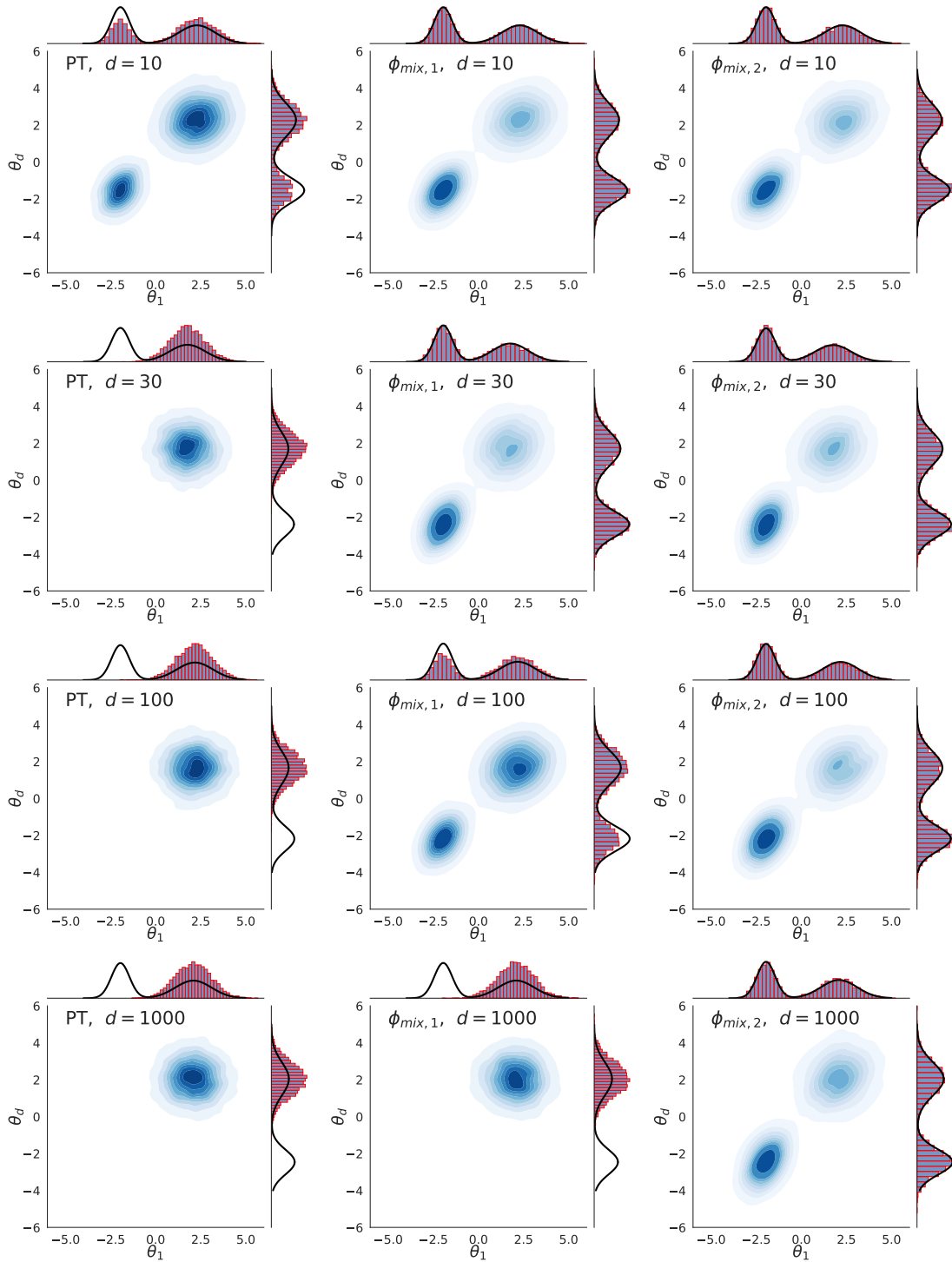


Fig. 9: Comparison of PT and Warp-U sampler in Setting 2. Each panel shows the density plot for  $(\theta_1, \theta_d)$ , which is drawn by one run of a MCMC sampler. Each panel also shows the marginal histogram for the Markov chain samples, and the black curves are the true marginal density. The three columns are for PT, Warp-U sampler with  $\phi_{mix,1}$  (see (41)), and Warp-U sampler with  $\phi_{mix,2}$  (see (42)), respectively. The four rows correspond to dimension  $d = 10, 30, 100$ , and  $1000$ , respectively.



**Table 3.** Summary statistics of the log target density evaluated at  $10^6$  samples, where the target density is a 10-dimensional mixed skew- $t$  distribution.

$\log(q)$	Min.	1st Qu.	Median	Mean	3rd Qu.	Max.
Target samples	-171.72	-27.86	-23.47	-24.67	-20.11	-10.26
Uniform samples	-53.07	-45.23	-43.71	-43.52	-42.01	-26.65

### 4.3. Comparison of Combined Sampling and Estimation Methods

We now compare our stochastic bridge estimation approach given by Algorithm 5 with bridge sampling (Meng and Wong, 1996) and Warp-U bridge estimation (Wang et al., 2022). The target density we consider is that used in Wang et al. (2022), and in particular is a 10 dimensional mixture of 25 multivariate skew- $t$  distributions whose mass mainly lies on the support  $[-20, 20]^{10}$ . A similar target density was first introduced in a simulation study designed by Azzalini (2013). The target density presents a challenge in that large regions of its support have low density. To illustrate this, we generated  $10^6$  samples first from the target density itself and then from a uniform distribution on  $[-20, 20]^{10}$ . In the case of the uniform samples, we found that 99.99% had target density value lower than one-hundredth of the median target density value of the samples directly obtained from the target density, see Table 3.

The three estimation methods we consider are all designed to estimate normalising constants *given* samples from the target density, and we investigate their performance when the samples are obtained via three different approaches: (i) our Warp-U MCMC sampler given by Algorithm 3; (ii) the Generalised Wang-Landau (GWL) algorithm (Liang, 2005); and (iii) PT. The GWL algorithm does not directly sample from the target density and therefore in the case of (ii) we apply the additional sub-sampling step suggested in Section 5.2 of Wang et al. (2022); see Section 6.1 for further discussion. We set the number of samples from the target density to be the same for all three sampling methods; specifically, we collect 26,000 samples under each method, as in Wang et al. (2022).

Figure 10 shows the root mean square error (RMSE) of the estimator as a function of the number of target evaluations for the classical bridge sampling (BS) estimator (green circles, and dash-dot line), the Warp-U bridge (WB) estimator (red triangles, and dotted line), and our stochastic Warp-U bridge (SWB) estimator (blue squares, and solid line), when the samples are provided by our adaptive Warp-U MCMC sampler (left), GWL (middle), and PT (right). Our stochastic bridge estimator has the smallest RMSE regardless of the sampling method used, except when the number of target evaluations is small. Whether using GWL or Warp-U MCMC samples, the results are similar and slightly better than with PT samples. On the other hand, GWL does not directly generate samples from the target distribution, and additional sub-sampling steps (see Section 5.2 of Wang et al. (2022)) are needed to get the target samples, so the total computational cost is higher than the other sampling methods (only the cost of estimation is illustrated in Figure 10).

We now return to Table 2 to compare the computational cost of the three estimation methods. In Table 2,  $M$  denotes the number of stages in our adaptive Warp-U MCMC sampler and the GWL algorithm, and  $M_l$  denotes the number of temperature levels for PT. For the GWL algorithm, the number of samples collected at each stage is different, so we use  $\bar{n}_1$  to denote the average number of samples across all stages (in practice,  $\bar{n}_1$  is relatively large compared with  $n_1$ ). In addition, burn-in is needed for all three sampling methods. Note that the number of iterations given in Table 2 is not necessarily the number of unique samples, because some proposed samples are rejected. Table 2 shows that classical bridge sampling and stochastic Warp-U bridge estimation both require no more computation than Warp-U bridge estimation, even when some estimation stage computation is saved by the use our Warp-U MCMC sampling method. The last row of Table 2 shows the computation cost of the three estimation methods given the samples, i.e., without considering the computation saved in the sampling stage. It shows that stochastic Warp-U bridge estimation required no more computation than Warp-U bridge estimation when all samples are given.

### 4.4. Warp-U Sampler Combined with an Unbiased Estimator

In Section 2.4 we introduced genuinely unbiased estimation strategies for the multi-modal distribution context which do not rely on checks for the convergence of the MCMC sampler. We now examine

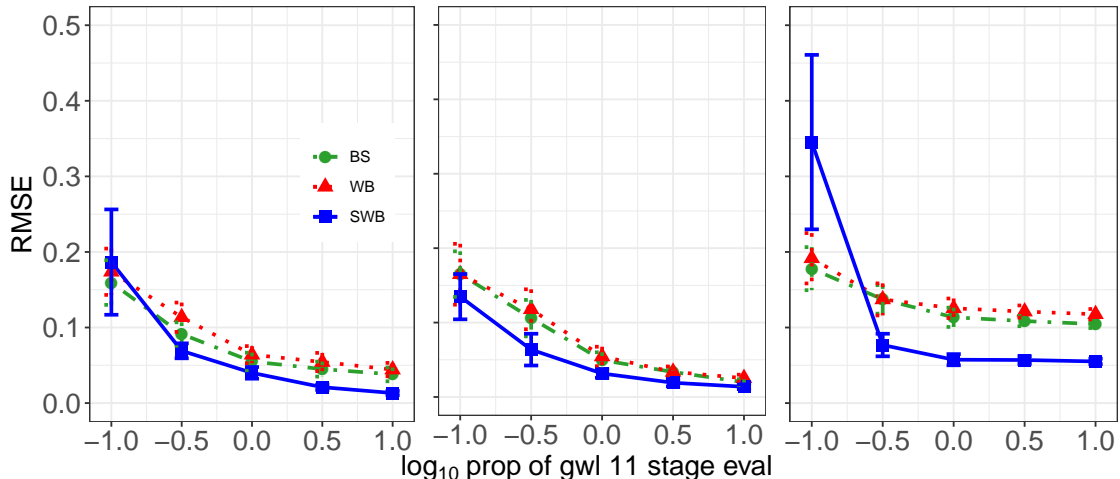


Fig. 10: Root mean square error (RMSE) of three normalising constant estimators as a function of the number of target evaluations, where the samples are obtained using our adaptive Warp-U MCMC sampler (left), GWL (middle), and PT (right). The three estimators are the classical bridge sampling (BS) estimator (green circles, and dash-dot line), the Warp-U bridge (WB) estimator (red triangles, and dotted line), and our stochastic Warp-U bridge (SWB) estimator (blue squares, and solid line). The error bars show 2 times the standard errors. The  $x$ -axis gives the number of estimation stage target evaluations as  $\log_{10}$  of the proportion of target evaluations needed for an 11th stage of the GWL algorithm.

the performance of these strategies, specifically the Warp-U unbiased estimation methods presented in Algorithm 4 (separate coupling for the Warp-U transformation and its inverse) and Algorithm S.3 (combined coupling). We also consider the three estimators (S.6)–(S.8) in the online Supplementary Material, which correspond to distinct levels of Rao-Blackwellization. The three estimators are denoted as L0, L1 and L2 respectively. L0 corresponds to the original estimator in (16)–(17) without Rao-Blackwellization. L1 exploits the conditional expectations  $\mathbb{E}[h(\theta_{1,t})|\theta_1^*]$  and  $\mathbb{E}[h(\theta_{2,t})|\theta_2^*]$  for Rao-Blackwellization, while L2 uses the conditional expectations  $\mathbb{E}[h(\theta_{1,t})|\theta_1^{\text{MH}}]$  and  $\mathbb{E}[h(\theta_{2,t})|\theta_2^{\text{MH}}]$ . See Section S.2 of the online Supplementary Material for more details. In this subsection we compare the six candidate methods corresponding to the two algorithms (Algorithm 4 and Algorithm S.3) and three levels of Rao-Blackwellization (L0, L1, and L2).

We consider two settings which are of higher dimension and more challenging than those in the previous subsections. In these two simulation settings, the target distribution is a mixture of multivariate Gaussian distributions and a mixture of multivariate skewed  $t$ -distributions (Gupta, 2003), respectively. In both settings there are 5 mixture components and the dimension of  $\theta$  is 30. The multivariate skewed  $t$ -distributions have 12 degree of freedom, and the elements of the skewness vector take values between  $-100$  to  $200$ . For the two mixture settings, density contours for the first 4 dimensions are plotted in Figure S.1 and Figure S.2 in the online Supplementary Material, respectively.

The high dimension of  $\theta$  makes it unlikely that the coupled chains will meet in the random walk Metropolis-Hastings step of Algorithm 4 and Algorithm S.3, which is consistent with the similar observations made by Jacob et al. (2020). Therefore, in our simulation study, all the random walk Metropolis-Hastings steps are replaced by the Hamiltonian Monte Carlo step proposed by Heng and Jacob (2019). The simulation is repeated 200 times for each setting.

Table 4 shows that the median meeting time ( $\tau := \inf\{t \geq 1 : \theta_{1,t} = \theta_{2,t-1}\}$ ) is less than 20 and 60 for the two settings, respectively. The combined Warp-U coupling scheme (Algorithm S.3) can further reduce the meeting time slightly, see rows two and four in Table 4. If we directly adopt the method of Jacob et al. (2020) without our Warp-U sampler, then the two chains generally get stuck in two different local modes and in

**Table 4.** Average value and 10%, 30%, 50%, 70%, 90% quantile for the meeting time  $\tau$  in the two mixture settings. Two Warp-U coupling schemes are compared: separate (Algorithm 4) and combined (Algorithm S.3).

Setting	Mixture Component	Warp-U Coupling	Average	10%	30%	50%	70%	90%
1	Gaussian	Separate	21.9	7	11	17	24	46
		Combined	20.8	7	10	16	24	40
2	Skewed $t$ -distribution	Separate	70.1	26	42	58	82	128
		Combined	62.9	26	36	52	74	115

practice are unlikely to meet at all. In conclusion, the proposed algorithms are effective for encouraging the meeting of the two chains in a multi-modal distribution context. Fast meeting of the two chains is important for the unbiased estimation scheme of Jacob et al. (2020) both theoretically and practically. Theoretically, the scheme requires the tail of the random meeting time to decay geometrically (see requirement R2 listed in Section 2.4). The practical side is that, after the two chains meet, we only need to run a single chain which saves computational resources.

The results of the first simulation setting (target distribution  $\pi$  is a mixture of Gaussian distribution) are shown in Figure 11. Specifically, Figures 11a–11b present the results for unbiased estimation of  $\mathbb{E}_\pi h(\theta)$  by  $H_{l:m}(\theta_{1,\cdot}, \theta_{2,\cdot})$  in (17), where  $h(\theta) = \sum_{j=1}^{50} \theta_j$ . The true value is  $\mathbb{E}_\pi h(\theta) \approx -4.786$ . Figures 11c–11d present the results for  $h(\theta) = \sum_{j=1}^{50} \theta_j^2$  with true value  $\mathbb{E}_\pi h(\theta) \approx 182.939$ .

In Figure 11a, the two rows correspond to  $l = 500$  and  $l = 1000$ , where  $l$  is the subscript of  $H_{l:m}(\theta_{1,\cdot}, \theta_{2,\cdot})$ . The first column contains the results of Algorithm 4, while the second column shows the results of Algorithm S.3. Each panel plots root mean squared error (RMSE) versus the number of iteration (i.e.  $m$  in the subscript of  $H_{l:m}$ ). In each panel, distinct curves represent different levels of Rao-Blackwellization (L0, L1 and L2). From the figure, we can find the estimation achieves high accuracy. Moreover, Rao-Blackwellization (L1 and L2) improves the accuracy over the original estimator (L0). The performance between L1 and L2 is similar. Meanwhile, the combined Warp-U coupling in Algorithm S.3 has accuracy close to the separate Warp-U coupling in Algorithm 4.

Figure 11b displays how RMSE decreases with computational time in seconds. The RMSE is computed for the estimator  $H_{l:m}$  with a proper value of  $m$ , such that the computational time falls within a certain time interval on the horizontal axis. Recall from Figure 11a that L1 and L2 levels of Rao-Blackwellization have similar performance as the number of iteration increases. However, in Figure 11b, RMSE for L2 decreases slower as the computation time increases. This is due to the heavier computational burden associated with L2, which requires  $K^2$  evaluations of the target  $q$ . On the other hand, L1 does not significantly increase the computational cost compared with the original estimator L0. This is because most of the necessary computation, which involves  $K$  evaluations of the target  $q$ , has already been completed during the Warp-U sampling phase. Our findings suggest that in most cases the L1 Rao-Blackwellization is as good or better than the L0 and L2 versions in terms of the computation time needed to reduce RMSE below a given threshold.

Lastly, Figure 11c–11d carry a similar message for the estimation of  $\mathbb{E}_\pi h(\theta)$  with  $h(\theta) = \sum_{k=1}^{50} \theta_k^2$ . The results of the second simulation setting (where the target distribution  $\pi$  is a mixture of multivariate skewed  $t$ -distribution) are shown in Figures S.3. The numerical results have a similar interpretation as those of the first setting.

#### 4.5. Sampling and Estimation in a Challenging 50-Dimensional Setting

To test the limit of the proposed method, we consider the 50 dimensional simulation setting in Section 4.3 of Wang et al. (2022). The target distribution  $\pi$  is a mixture of 30 distributions, including normal distributions,  $t$ -distributions (including Cauchy distributions), and multivariate distributions with gamma and/or exponential marginal distributions and normal copulas. In the work of Wang et al. (2022), independent and identically distributed samples are drawn from  $\pi$  and fed to the Warp-U bridge estimator. In this subsection, we endeavour to draw samples via our proposed adaptive Warp-U MCMC sampler (Algorithm 3) and then estimate the normalising constant.

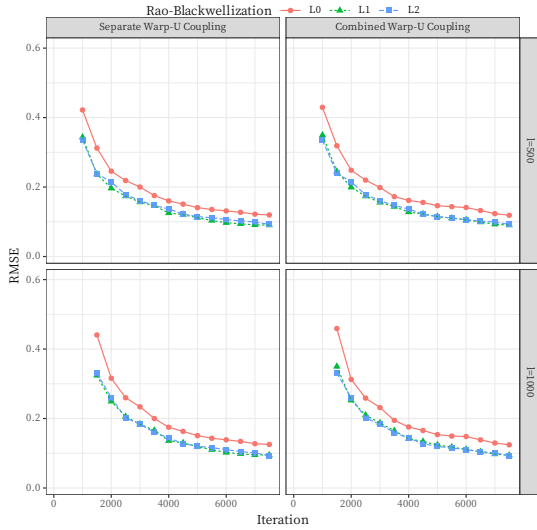
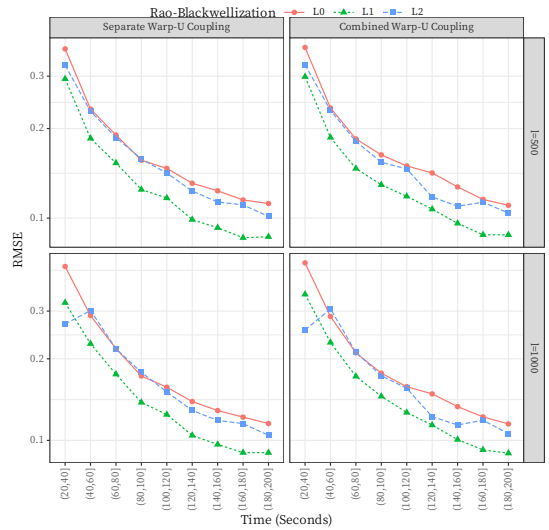
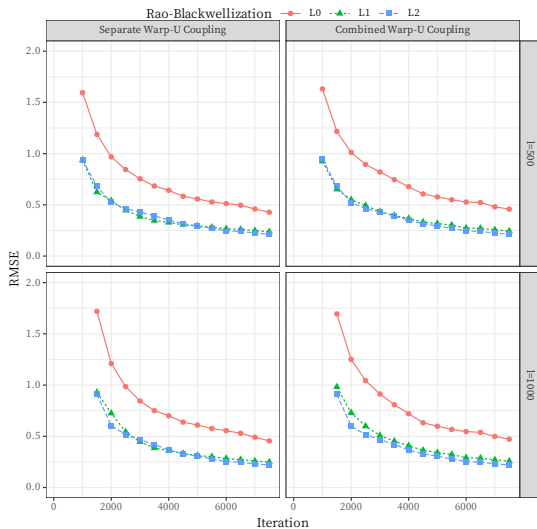
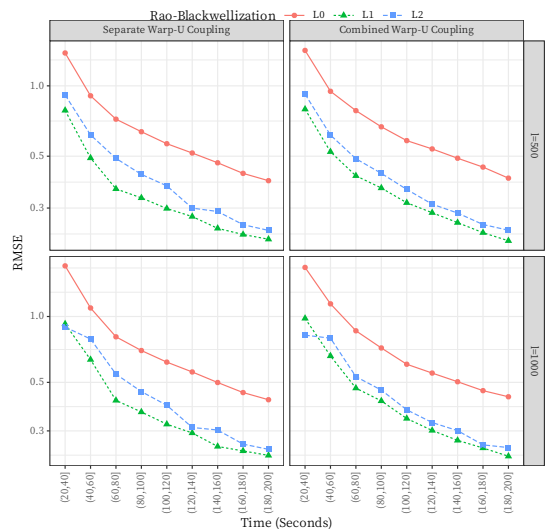
(a) RMSE vs. Iteration with  $h(\theta) = \sum_{j=1}^{50} \theta_j$ .(b) RMSE vs. Computation Time with  $h(\theta) = \sum_{j=1}^{50} \theta_j$ .(c) RMSE vs. Iteration with  $h(\theta) = \sum_{j=1}^{50} \theta_j^2$ .(d) RMSE vs. Computation Time with  $h(\theta) = \sum_{j=1}^{50} \theta_j^2$ .

Fig. 11: Unbiased estimation of  $\mathbb{E}_\pi h(\theta)$  by  $H_{l:m}(\theta_{1,\cdot}, \theta_{2,\cdot})$  where  $\pi$  is a mixture of Gaussian distribution. In Figure 11a and Figure 11b,  $h(\theta) = \sum_{j=1}^{50} \theta_j$ . In Figure 11c and Figure 11d,  $h(\theta) = \sum_{j=1}^{50} \theta_j^2$ . Figure 11a and Figure 11c show root mean squared error (RMSE) versus the number of iteration (i.e.  $m$  in  $H_{l:m}(\theta_{1,\cdot}, \theta_{2,\cdot})$ ); Figure 11b and Figure 11d shows root mean squared error (RMSE) versus computational time (seconds). For each subfigure, the two rows of panels correspond to  $l = 500$  and  $l = 1000$  (i.e.  $l$  in the notation  $H_{l:m}(\theta_{1,\cdot}, \theta_{2,\cdot})$ ), respectively. The first column presents the result of Algorithm 4, while the second column shows the results of Algorithm S.3. Distinct curves represent different levels of Rao-Blackwellization: L0, L1 and L2.

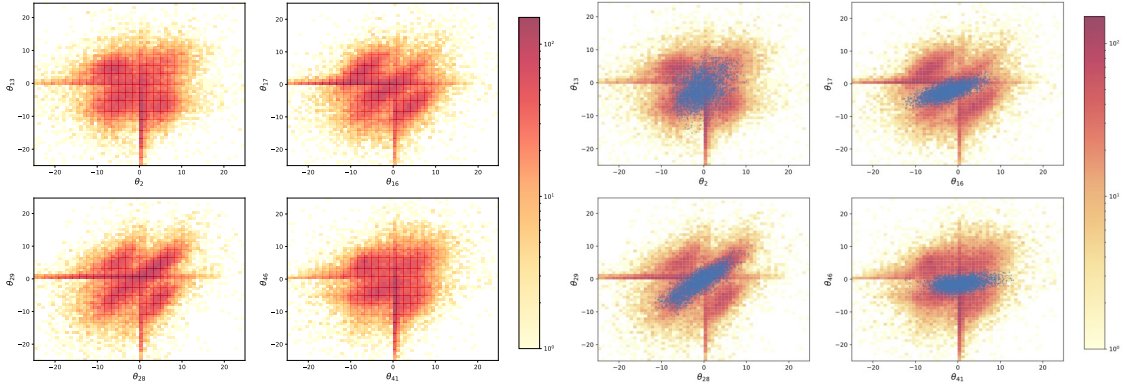


Fig. 12: Left panel: two-dimensional histogram of i.i.d. samples from the target distribution for some selected pairs of dimensions. Right panel: Warp-U MCMC samples (blue points) with a  $\phi_{\text{mix}}$  whose mixture component mean vectors are drawn from a uniform distribution.

The left panel of Figure 12 shows marginal two-dimensional histograms of i.i.d. samples from the target distribution. Because the target distribution contains Cauchy distributions and  $t$ -distributions as its mixture components, some i.i.d. samples take extreme values. The plot only shows the density around the origin. Since the target distribution has heavy tails and complex density contours in 50 dimensions, obtaining samples from the target distribution using MCMC is very challenging. Direct application of the adaptive Algorithm 3 with the basic sampler in Algorithm 2 will not work effectively. One obstacle is that in 50 dimensions the random walk Metropolis Hastings step in Algorithm 2 is ineffective, and therefore needs to be replaced by a Hamiltonian Monte Carlo (HMC) step. Even with this replacement, the Warp-U sampler can still get stuck in local modes.

For illustration, we set the auxiliary distribution  $\phi_{\text{mix}}$  to have  $K = 200$  components. We initialise  $\phi_{\text{mix}}(\theta)$  by drawing its mean vector  $\mu_k$  from a uniform distribution  $\text{Uniform}([-15, 15]^{50})$ , and setting the covariance matrix of each mixture component of  $\phi_{\text{mix}}(\theta)$  to be  $3I$ . Lastly, we set the mixture components of  $\phi_{\text{mix}}(\theta)$  to have equal weights, i.e.  $w_k = 1/K$ . This is a typical  $\phi_{\text{mix}}(\theta)$  to choose when we have little prior knowledge about the target distribution before the adaptive algorithm begins. The resulting Warp-U MCMC samples are shown in the right panel of Figure 12. The figure indicates the Warp-U sampler with this initial  $\phi_{\text{mix}}(\theta)$  fails to explore the full sample space.

The reason that Warp-U transformation fails to shift samples across modes can be explained by Figure 13. In the left panel, the black point is a sample  $\theta^{\text{HMC}}$  generated by the HMC step. The Warp-U transform and its inverse essentially propose to shift  $\theta^{\text{HMC}}$  to one of the following points

$$\theta_{\psi, \psi'} = \mathcal{H}_{\psi'} \circ \mathcal{F}_{\psi}(\theta^{\text{HMC}}) = \theta^{\text{HMC}} - \mu_{\psi} + \mu_{\psi'}, \quad \psi, \psi' = 1, 2, \dots, K.$$

Among these  $K^2 = 40,000$  candidates, 200 candidates (with a fixed  $\psi$  and  $\psi' = 1, \dots, 200$ ) are shown as blue points in the right panel. The logarithm of the target density  $\log \pi(\theta_{\psi, \psi'})$  at all 40,000 candidates (with  $\psi, \psi' = 1, \dots, 200$ ) is shown in the right panel of Figure 13. We can see the density at  $\psi = \psi'$  is much larger than for  $\psi \neq \psi'$ . This indicates that for  $\psi \neq \psi'$  the Warp-U transformation usually shifts the current  $\theta^{\text{HMC}}$  to a low density region. Therefore, with  $\phi_{\text{mix}}(\theta)$  constructed as described above, the Warp-U sampler only chooses the identity transformation  $\mathcal{H}_{\psi} \circ \mathcal{F}_{\psi}(\theta^{\text{HMC}}) = \theta^{\text{HMC}}$  (with  $\psi = \psi'$ ), and so the resulting Markov chain fails to jump efficiently between modes.

To overcome the above issue, we consider a further modification of the basic sampler (Algorithm 2) to encourage sample space exploration in the early stages of adaptive Warp-U (Algorithm 3). The modified version of Algorithm 2 is presented in Algorithm S.5 in the online Supplement Material. This version of

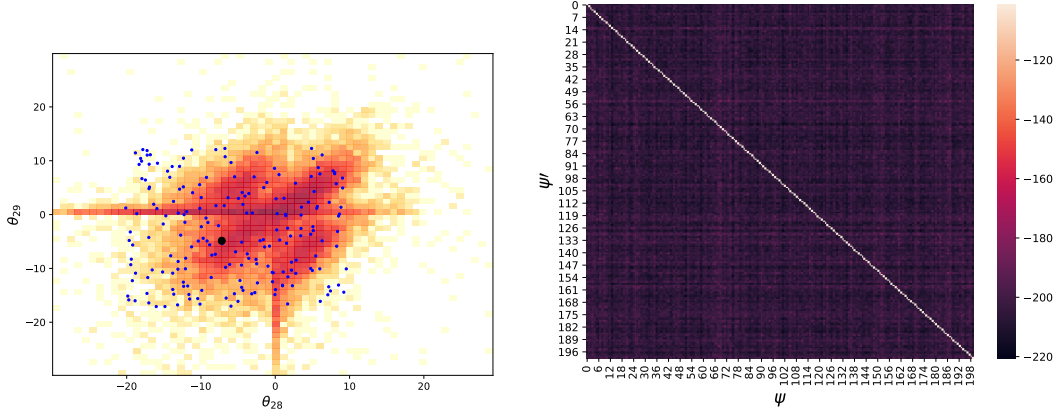


Fig. 13: The Warp-U transformation and its inverse tries to shift the current sample to one of  $\mathcal{H}_{\psi'} \circ \mathcal{F}_{\psi}(\boldsymbol{\theta}^{\text{HMC}})$  ( $\psi, \psi' = 1, 2, \dots, 200$ ). Left panel: the black point is the current sample  $\boldsymbol{\theta}^{\text{HMC}}$ , and the blue points represent 200 candidates with a fixed  $\psi$  and  $\psi' = 1, \dots, 200$ . The background is the two-dimensional histogram for i.i.d. samples. Right panel: the heatmap of  $\log(\pi(\mathcal{H}_{\psi'} \circ \mathcal{F}_{\psi}(\boldsymbol{\theta}^{\text{HMC}})))$  for all the 400,00 candidate points with  $\psi, \psi' = 1, 2, \dots, 200$ .

algorithm draws the inverse Warp-U transformation  $\mathcal{H}_{\psi'}$  with probability

$$\tilde{\nu}(\psi' | \boldsymbol{\theta}^*) \propto \exp \{ \log(\nu(\psi' | \boldsymbol{\theta}^*)) / C^{(s)} \},$$

instead of  $\nu(\psi' | \boldsymbol{\theta}^*)$  in Line 5 of Algorithm 2. The constant  $C^{(s)} (\geq 1)$  forces the probability towards a uniform distribution, which is similar to the simulated annealing strategy. We investigate combining Algorithm 3 with Algorithm S.5, instead of Algorithm 2. As the adaptive stage  $s$  increases in Algorithm 3, the constant  $C^{(s)} (\geq 1)$  is gradually decreased to 1. In the final stages, we set  $C^{(s)} = 1$  and Algorithm S.5 reduces to the original version of basic Warp-U sampler (i.e. Algorithm 2 except with an HMC proposal). See Section S.7 of the online Supplementary Material for more details of Algorithm S.5.

To further assist local mode exploration in the adaptive stage, we adopted the following auxiliary distribution

$$\phi_{\text{mix}} = 0.5\phi_{\text{mix}}^{(\text{adapt.})} + 0.5\phi_{\text{mix}}^{(\text{opt.})}. \quad (43)$$

In the above,  $\phi_{\text{mix}}^{(\text{opt.})}$  is a mixture distribution with 11 mixture components. Its centres are found via optimisation: specifically, we ran an optimisation algorithm with 2,000 random initial points and 11 unique local maxima were detected. As before, each mixture component of  $\phi_{\text{mix}}^{(\text{opt.})}$  has equal weight and diagonal covariance matrix  $3I$ . The distribution  $\phi_{\text{mix}}^{(\text{adapt.})}$  is fitted adaptively to MCMC samples as Algorithm 3 proceeds, while  $\phi_{\text{mix}}^{(\text{opt.})}$  is fixed. This choice of  $\phi_{\text{mix}}$  and its mixture weights is arbitrary and not optimised, but is sufficient to illustrate the benefits of this approach in our empirical studies, which we now describe.

For the 50 dimensional target distribution, we compare the Warp-U bridge and stochastic Warp bridge estimation under three specific settings based on the discussion above. The settings are summarized in Table 5. In the i.i.d. setting, the auxiliary distribution  $\phi_{\text{mix}}^{(\text{i.i.d.})}$  is obtained by applying the EM algorithm to 30,000 i.i.d. samples; meanwhile, an independent set of 10,000 i.i.d. samples are fed to the bridge estimators. In the setting HMC+WarpU(i.i.d.), the auxiliary distribution is chosen as  $0.5\phi_{\text{mix}}^{(\text{i.i.d.})} + 0.5\phi_{\text{mix}}^{(\text{opt.})}$ , where  $\phi_{\text{mix}}^{(\text{i.i.d.})}$  is the Gaussian mixture fitted to i.i.d. samples, and  $\phi_{\text{mix}}^{(\text{opt.})}$  is the Gaussian mixture whose centres are found by optimisation. In the setting HMC+WarpU(adaptative), we use  $0.5\phi_{\text{mix}}^{(\text{adapt.})} + 0.5\phi_{\text{mix}}^{(\text{opt.})}$  in (43) as the auxiliary distribution. For both HMC+WarpU(i.i.d) and HMC+WarpU(adaptative), we run Algorithm S.5 with  $C^{(s)} = 1$  to generate 10,000 MCMC samples during the last adaptive stage. These MCMC samples are then supplied to the bridge estimators.

**Table 5.** Settings for the bridge estimator. The auxiliary  $\phi_{\text{mix}}^{(\text{i.i.d.})}$  is fitted by i.i.d. samples by EM algorithm,  $\phi_{\text{mix}}^{(\text{opt.})}$  is a mixture of Gaussian whose centres are local modes detected by optimisation. The auxiliary  $\phi_{\text{mix}}^{(\text{adapt})}$  is fitted to the adaptive Warp-U samples.

Setting	$\phi_{\text{mix}}$	Samples for bridge estimators
i.i.d.	$\phi_{\text{mix}}^{(\text{i.i.d.})}$	i.i.d samples
HMC+WarpU(i.i.d.)	$0.5\phi_{\text{mix}}^{(\text{i.i.d.})} + 0.5\phi_{\text{mix}}^{(\text{opt.})}$	Warp-U MCMC samples with HMC proposal
HMC+WarpU(adaptive)	$0.5\phi_{\text{mix}}^{(\text{adapt})} + 0.5\phi_{\text{mix}}^{(\text{opt.})}$	Warp-U MCMC samples with HMC proposal

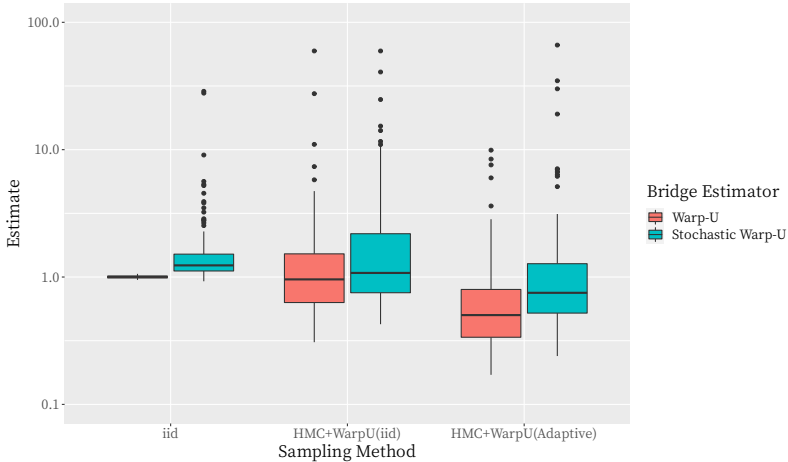


Fig. 14: Warp-U bridge and stochastic Warp-U bridge estimation of the normalising constant under 100 simulation replicates. The true value of the normalising constant is 1. From left to right, the boxplots are divided into three groups. See Table 5 for the specific setting of each group.

For HMC+WarpU(i.i.d) and HMC+WarpU(adaptive), the samples generated by one run of the modified algorithm are shown in Figure S.4 and Figure S.5 in the online Supplement Material, respectively. With a properly fitted  $\phi_{\text{mix}}$ , the Warp-U sampler is capable of exploring multiple modes in this complex high dimensional setting.

The estimation of the normalising constants under 100 replicates is shown in Figure 14. The true value of the normalising constant is 1. The leftmost boxplot indicates the Warp-U bridge estimator with i.i.d sample provides a very accurate estimation, which is consistent with the work of Wang et al. (2022). The next boxplot shows the stochastic Warp-U bridge estimator with i.i.d. samples has a slightly larger estimation error. This is because the stochastic Warp-U bridge estimator requires that each transformed density matches the standard Gaussian distribution, and this requirement is difficult to meet for the current target distribution with complex density contours and heavy tails. Under the HMC+WarpU(i.i.d) and HMC+WarpU(adaptive) settings, the estimation of the normalising constant is close to 1 in most simulation replicates. A few replicates produce estimates close to 100.

The computational findings presented in this subsection demonstrate that our proposed adaptive sampler might struggle to perform efficiently when faced with high-dimensional distributions with complex density contours. During the initial adaptive phase,  $\phi_{\text{mix}}$  is initialized with random guessing, which can result in Warp-U transformations failing to shift the Markov chain to a different high-density region. To mitigate this issue, we combined the concept of simulated annealing with the Warp-U transformations, which facilitates sample space exploration in the early stages. Despite the tactics applied within this subsection, the derived  $\phi_{\text{mix}}$  does not precisely emulate the target distribution. A potential avenue for future research is to develop other variational inference techniques (Arenz et al., 2020; Yan et al., 2023) to fit a high-quality  $\phi_{\text{mix}}$  from the onset. Additionally, the efficiency of local exploration around individual local modes is compromised due to

the inefficiency of Hamiltonian Monte Carlo (HMC) when sampling densities with highly irregular density contours and heavy tails (Hoffman et al., 2019; Livingstone et al., 2019). These limitations could be the reason why the Warp-U samples used in the bridge estimators have failed to deliver highly accurate estimates of the true normalizing constant.

## 5. Exoplanet Detection Using Radial Velocity (RV) Data

In astronomy, one of the most successful approaches for detecting exoplanets is the radial velocity (RV) method (exoplanets are planets outside our Solar System). The radial velocity of a star is its velocity towards or away from the Earth in meters per second (m/s). When an exoplanet orbits a star, the gravitational force of the planet impacts the RV of the star, and RV data can therefore be used to detect exoplanets. Consider a candidate model  $\mathcal{M}$  for capturing the physical system and noise, e.g.,  $\mathcal{M}$  might be a Keplerian model for a single exoplanet orbiting a star with Gaussian measurement noise. From a Bayesian perspective, it is natural to compute the Bayesian evidence of the model  $\mathcal{M}$ :

$$\mathcal{Z} \equiv p(\mathbf{d}|\mathcal{M}) = \int p(\mathbf{d}|\boldsymbol{\theta}, \mathcal{M})p(\boldsymbol{\theta}|\mathcal{M})\mu(\mathrm{d}\boldsymbol{\theta}), \quad (44)$$

where  $\mathbf{d}$  is the RV data and  $\boldsymbol{\theta}$  denotes the parameters of  $\mathcal{M}$ . Here  $p(\mathbf{d}|\boldsymbol{\theta}, \mathcal{M})$  is the likelihood function and  $p(\boldsymbol{\theta}|\mathcal{M})$  as the prior. The Bayesian evidence  $\mathcal{Z}$  is the normalising constant of the posterior distribution of  $\mathbf{d}$  given up to proportionality by  $\propto p(\mathbf{d}|\boldsymbol{\theta}, \mathcal{M})p(\boldsymbol{\theta}|\mathcal{M})$ , and represents the evidence in support of the model  $\mathcal{M}$ . Consider the following model for the observed RV  $v_i$  at time  $t_i$ :

$$v_i = v_{\text{pred}}(t_i|\boldsymbol{\theta}) + \epsilon_i, \quad (45)$$

where  $v_{\text{pred}}$  is a Keplerian model for the planetary system (see Danby, 1988; Loredo et al., 2012),  $\boldsymbol{\theta}$  denotes the physical parameters, and  $\epsilon_i$  is a noise term. Further details of the physical model are given in Section S.6 of the online Supplementary Material. One important statistical feature of RV data is that the noise exhibits correlation across observations. In accordance with Rajpaul et al. (2015) and Jones et al. (2022), we make the assumption that this noise follows a Gaussian process, i.e.,  $\boldsymbol{\epsilon} \sim \mathcal{N}(\mathbf{0}, \boldsymbol{\Sigma})$ . We model the covariance matrix  $\boldsymbol{\Sigma}$  by

$$\boldsymbol{\Sigma}_{ij} = \kappa_{ij} + \delta_{ij}(\sigma_i^2 + \sigma_L^2), \quad (46)$$

where  $\kappa_{ij}$  is a quasi-periodic kernel,  $\delta_{ij}$  is the Kronecker delta,  $\sigma_i^2$  is the variance due to measurement error, and  $\sigma_L^2$  captures additional variation. The quasi-periodic kernel is given by

$$\kappa_{ij} = \alpha^2 \exp \left[ -\frac{1}{2} \left\{ \frac{\sin[\pi(t_i - t_j)/\tau]}{\lambda_p^2} + \frac{t_i - t_j}{\lambda_e^2} \right\}^2 \right], \quad (47)$$

and the kernel hyperparameters treated as known in our dataset (described below) are fixed at  $\alpha = \sqrt{3}$  meters/second,  $\lambda_e = 50.0$  days,  $\lambda_p = 0.5$  (unit-less), and  $\tau = 20$  (days).

Our dataset consists of  $n = 200$  simulated observations from the Extremely Precise Radial Velocities (EPRV3) Evidence Challenge which compared Bayesian evidence estimates produced by different statistical methods in the context of RV exoplanet detection; see Nelson et al. (2020) for details. Each observation is accompanied by the time at which the RV is measured and a known measurement error (i.e., standard deviation). The data are plotted in the left panel of Figure 15.

### 5.1. Comparison with Parallel Tempering and Hamiltonian MC

We compare the performance of our adaptive Warp-U MCMC sampler to that of PT and Hamiltonian Monte Carlo (HMC) (see Betancourt and Girolami, 2015; Neal et al., 2011), in terms of its ability to recover the marginal posterior distribution of the *Mean Anomaly* physical parameter used in the Keplerian model introduced in (45) and Section S.6 of the online Supplementary Material. The Hamiltonian Monte Carlo sampling is performed using the `RStan` package; see Stan Development Team (2019) and Stan Development



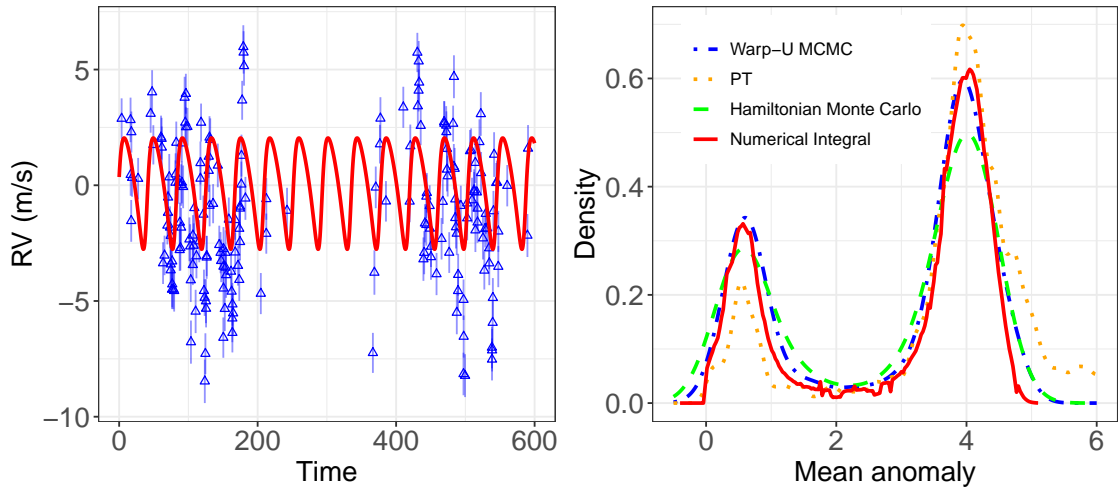


Fig. 15: The left panel shows the true radial velocity signal as a function of time (solid red line), and observed measurements and their associated measurement errors  $\sigma_i^2$  (blue triangles and vertical bars). Note that the measurement errors represent errors typically reported by an observing telescope, and as can be seen in (46) and the left panel they do not account for all uncertainties. The right panel shows the marginal posterior distribution of the mean anomaly parameter. It compares the estimated densities using the samples obtained by Warp-U MCMC (dash-dot blue line), PT (dotted orange line) and HMC (dashed green line). The solid red line is the estimated target density by the numerical integral.

**Table 6.** RMSE (and associated SE) when estimating the  $\log_{10}$  Bayesian evidence for a planet using bridge sampling, Warp-U bridge estimation, and stochastic Warp-U bridge estimation.

Sampling	Bridge		Warp-U		S. Warp-U	
	RMSE	SE	RMSE	SE	RMSE	SE
PT	0.238	0.015	0.239	0.017	0.115	0.008
Warp-U	0.136	0.004	0.137	0.008	0.059	0.002

Team (2020). We focus on the *Mean Anomaly* because its posterior distribution is expected to be multimodal. The temperature grid needed for PT was tuned via the algorithm proposed in Atchadé et al. (2011). To obtain a baseline for comparison, we also applied brute-force numerical integration (at a high computational cost) to obtain the true posterior distribution of the model parameters. The right panel of Figure 15 compares the marginal posterior distribution of the *Mean Anomaly* obtained under the three different sampling methods. The figure demonstrates that our adaptive Warp-U MCMC sampler more accurately recovers the marginal posterior distribution than PT and HMC. It is also worth noting that PT required substantial tuning, whereas our Warp-U MCMC method did not (the Stan package automatically ran tuning required for HMC).

## 5.2. Estimation of the Bayesian Evidence

Next, we compare the performance of stochastic Warp-U bridge estimation with standard bridge sampling estimation and Warp-U bridge estimation. We first applied PT and our adaptive Warp-U MCMC sampler to get the target samples needed by the estimation methods. To make the comparison fair, the total number of evaluations of the target density across the sampling and estimation steps is set to be the same for all the methods.

Following Nelson et al. (2020), we use the median value of the Bayesian evidence obtained across all the methods investigated in the Extremely Precise Radial Velocities (EPRV3) Evidence Challenge as the

quasi true value (i.e.,  $\log_{10}(\hat{c}) = -193.71$ ). Table 6 compares the root mean square error (RMSE) for bridge sampling, Warp-U bridge estimation, and stochastic Warp-U bridge estimation. The RMSE is the smallest under our stochastic Warp-U bridge estimation method. Table 6 also shows that the RMSE is lower when the target samples are obtained by our adaptive Warp-U MCMC sampler than when they are obtained via PT, which again illustrates the benefits of our sampling method. Our closest estimate to the quasi-true value was  $\log_{10}(\hat{c}) = -193.74$ , and was obtained by stochastic Warp-U bridge estimation using the samples from Warp-U MCMC sampler. Based on the bias shown in Nelson et al. (2020), which ignores the variance and therefore represents the methods in Nelson et al. (2020) favourably, our stochastic Warp-U bridge estimator utilising samples from the Warp-U MCMC sampler has an RMSE that is comparable to the best methods investigated in the EPRV3 Evidence Challenge. Lastly, note that the standard errors of the RMSE in Table 6 are smaller under our stochastic Warp-U bridge estimation strategy.

## 6. From Past to the Future

### 6.1. A brief Overview of Comparable Methods

Many algorithms have been developed to sample from multi-modal densities, a number of which simultaneously perform sampling and estimation of normalising constants. A leading example of the latter category of techniques is the Generalised Wang-Landau (GWL) algorithm proposed by Liang (2005), which is an energy based adaptive importance sampling method. The multi-stage approach used in our adaptive method was inspired by the GWL algorithm, and earlier adaptive importance sampling strategies such as Liang (2002), Berg and Neuhaus (1991), and Wang and Landau (2001). There have been several extensions to the GWL algorithm, including Liang et al. (2007) and Bornn et al. (2013), but also some concerns about its convergence properties. Jacob et al. (2014) showed that only some variations reach the so-called flat histogram convergence criterion in finite time, whereas other variations do not. Furthermore, Wang et al. (2022) illustrated that the GWL normalising constant estimator is sometimes inefficient, and the alternative strategy of applying Warp-U bridge estimation to the GWL draws (after weighted resampling) can substantially reduce RMSE (for fixed computational resources).

Indeed, although it is conceptually appealing to combine sampling and estimation in a single step, existing techniques for performing these tasks separately are in some ways more developed. Some existing algorithms also apply the idea of transporting the mass of the target density, e.g., Parno and Marzouk (2018) constructs transport maps to match the target distribution and a reference distribution for more efficient Metropolis-Hasting proposal. Some theory regarding the optimal transformation has been developed by Villani (2003). Pompe et al. (2020) proposed a sampling method that begins by finding the modes of the target distribution via optimization; then, based on this knowledge of the mode locations, they augment the parameter space with a mode index and generate samples via a combination of local moves and mode-jumping moves. Their mode-jumping moves are based on the Metropolis-Hastings algorithm, whereas in our algorithm mode-jumping is achieved via Warp-U transformations. Tak et al. (2018) proposed a repelling-attracting Metropolis-Hastings (RAM) algorithm for exploring multi-modal distributions; it works by constructing a proposal distribution which combines a move to low density and a move back to high density.

Perhaps the best known general strategy for sampling from multi-modal densities is parallel tempering (Geyer, 1991). Recent studies (Syed et al., 2021, 2022; Surjanovic et al., 2022) proposed more efficient version parallel tempering, focusing on its integration with a variational reference distribution, the implementation of flexible annealing paths, and the adoption of non-reversible communication schemes. Since parallel tempering is a sampling algorithm, it needs to be combined with an estimation strategy, e.g., bridge sampling. In our simulation studies, we find that our proposed strategy is computationally more efficient than parallel tempering for two reasons: firstly, more of the computation for the estimation step is performed by our Warp-U sampler than by parallel tempering, and secondly, the Warp-U sampler involves only one chain and it always accepts inter-mode proposals.

Of course, it would be foolish to suggest Warp-U sampler dominates parallel tempering (and other methods) for all cases, but the evidence we have accumulated so far does suggest that it is a viable alternative in terms of both computational cost and implementation effort. The experiments in Section 4.2 also indicate that the

Warp-U sampler has the potential to surpass parallel tempering in efficiency, particularly when dealing with target distributions that are high-dimensional and feature modes with different variances.

## 6.2. Limitations and Further Work

Whereas our overall approach is generally simple to implement because fitting mixture distributions is typically straightforward (and easy to interpret), a limitation is that the number of components in the mixture,  $K$ , has to be chosen (or inferred), and further research is needed on optimally determining this number without unduly increasing computational cost. Nevertheless, in our limited study so far, we find that our approach is rather robust to  $K$  as long as it is not too small. Thus, with adequate computational resources, one can avoid tuning by setting the number of components to be high initially. Specifically, in many settings, starting with a moderate number of components, e.g.,  $K = 20$ , is practical. If the target density has fewer than  $K$  modes, this will not substantially negatively impact the performance of the sampling method, and the main price of specifying too many components is the computational cost of updating the Gaussian mixture approximation  $\phi_{\text{mix}}$ . It may be worthwhile to use a model selection criterion, e.g., BIC, to determine  $K$ , and we encourage interested readers to explore and investigate the performance of our methods as they adopt different methods for choosing  $K$ .

A more serious limitation of our adaptive Warp-U MCMC sampler is that it is likely inefficient in the case of very isolated modes, partly because it may take time to identify the modes, and partly because its advantages over a Metropolis-Hastings (MH) algorithm with a mixture density proposal rely on the overlap between modes, and is diminished in the case of isolated modes. On the other hand, sampling from isolated modes with unknown locations is universally challenging. A possible strategy is to combine several methods to take advantage of their different strengths, similar to the interweaving strategy in Yu and Meng (2011). For example, one could consider implementing the Warp-U sampler within each chain of PT, or even consider using some warp transformation parameters themselves as temperature parameters to be adaptively varied as the overall interwoven algorithm iterates. Such interwoven algorithms would undoubtedly lose the simplicity of the Warp-U sampler or of PT, but with the payoff of overcoming challenges that may defeat the individual algorithms. Of course, much research is needed to explore such ideas.

The experiment in Section 4.5 also reveals limitations of the proposed adaptive Warp-U sampler, especially when applied to intricate, high-dimensional target densities. However, these limitations can possibly be mitigated by initializing a high-quality  $\phi_{\text{mix}}$  using variational inference (Arenz et al., 2020; Yan et al., 2023). The experiment further underscores that, even when substituting the random walk Metropolis step with a Hamiltonian step, the algorithm might still exhibit inefficiencies in high-dimensional local exploration. This is primarily attributed to the target density’s irregular contour and heavy tail. The prevalent literature offers solutions to the challenge posed by irregular density contours, primarily through density transformation (Hoffman et al., 2019) or adaptation based on local geometry (Girolami and Calderhead, 2011). The Warp-U transformation again provides a promising alternative: instead of directly sampling from the original target  $\pi$  to explore locally, one could employ the Hamiltonian step to draw from the Warp-U transformed  $\tilde{\pi}$ , which resembles a Gaussian distribution and exhibits more regularity. Subsequently, the inverse Warp-U transformation can be applied to get samples from  $\pi$ . This is similar to the approach proposed in Algorithm 1 of Parno and Marzouk (2018). On the other hand, the challenge posed by heavy-tailed densities could possibly be solved by more sophisticated local proposals, e.g., local proposals with jumps (Şimşekli, 2017).

We also want to point out that in stochastic Warp-U bridge sampling estimation, when allocating the samples to different components in Steps 3–4 of Algorithm 5, there may be some components that have very few samples, which will lead to high variance of the bridge sampling estimator for those components. To address this problem, future work could develop a restriction to ensure that each component has a minimum number of samples, or by adaptively merging components to ensure sufficient mass for each component. However, such merges may decrease the quality of the fit of the mixture model, leading to (practical) higher bias, at least when the chains are still in the exploratory stage. Therefore, much research is needed to investigate this issue and to provide theoretically sound practical guidelines on how to deal with such a bias-variance trade-off.

In the current work, we separately address two distinct estimators: the stochastic Warp-U bridge estimator for estimating the normalizing constant, and Warp-U sampling with an unbiased estimator for estimating

$\mathbb{E}_\pi h(\boldsymbol{\theta})$  for a general function  $h$ . A potential avenue for future research could involve integrating these two estimators. For example, the unbiased strategy can be applied to estimate the denominator of the bridge estimator (see (20)).

The current unbiased estimation strategy is limited by its incurred computational cost. Before the two chains meet, the computational cost is more than double that of a single chain, because we need to compute the joint transition kernel and draw samples from it. The additional cost can be significant for a complex  $q$  and a large number of mixture component  $K$ . Moreover, in Section 2.4, we use optimal transport coupling to find the joint transition kernel for the Warp-U transformation step and its inverse step. This strategy minimizes the expected distance between the two chains and is similar to Papp and Sherlock (2022). Understanding the limiting behaviour of this coupling in high dimension and developing other coupling is also a possible direction for future research.

Last but not the least, much needs to be done to address the biggest theoretical gap in our current article. That is, the theoretical comparisons we made about asymptotic variance or precision per CPU second are under the assumption of i.i.d. draws, which is clearly violated by our algorithm and other MCMC methods we used in this article. Whereas more painstaking efforts to extend the results to dependent draws are certainly possible, the more ideal approach is to implement Warp-U sampler perfectly (which *would* produce i.i.d. draws), in the sense of the perfect sampling made possible by the seminal work of Propp and Wilson (1996). Unfortunately, implementing perfect sampling is typically a daunting task, and often impractical; see Craiu and Meng (2011) for an overview and discussion. However, for our Warp-U sampler, the mixture component index  $\phi$  is discrete, which opens the door for inducing practically feasible coalescence that is critical for implementing perfect sampling; see for example, Stein and Meng (2013), who implemented perfect sampling for the common Dirichlet-multinomial model by utilising the discreteness of the mixture index. This is definitely a worthwhile direction for further research; it will require hard work, especially for the adaptive version of the Warp-U sampler, but the potential reward is large.

## Acknowledgements

We thank Yves Atchade and Pierre Jacob for very helpful comments, and US NSF for partial financial support (to XLM).

## Supplementary Material

Supplementary Materials are available online, containing technical proofs, the details of the unbiased Warp-U estimator and additional numerical results.

## References

- S. M. Ali and S. D. Silvey. A general class of coefficients of divergence of one distribution from another. *Journal of the Royal Statistical Society: Series B (Methodological)*, 28(1):131–142, 1966.
- C. Andrieu and C. P. Robert. *Controlled MCMC for optimal sampling*. INSEE, 2001.
- O. Arenz, M. Zhong, and G. Neumann. Trust-region variational inference with gaussian mixture models. *The Journal of Machine Learning Research*, 21(1):6534–6593, 2020.
- Y. F. Atchadé. An adaptive version for the metropolis adjusted langevin algorithm with a truncated drift. *Methodology and Computing in applied Probability*, 8(2):235–254, 2006.
- Y. F. Atchadé, G. O. Roberts, and J. S. Rosenthal. Towards optimal scaling of metropolis-coupled markov chain monte carlo. *Statistics and Computing*, 21(4):555–568, 2011.
- A. Azzalini. *The skew-normal and related families*, volume 3. Cambridge University Press, 2013.
- C. H. Bennett. Efficient estimation of free energy differences from monte carlo data. *Journal of Computational Physics*, 22(2):245–268, 1976.
- B. A. Berg and T. Neuhaus. Multicanonical algorithms for first order phase transitions. *Physics Letters B*, 267(2):249–253, 1991.
- M. Betancourt and M. Girolami. Hamiltonian monte carlo for hierarchical models. *Current trends in Bayesian methodology with applications*, 79(30):2–4, 2015.

- N. Biswas, P. E. Jacob, and P. Vanetti. Estimating convergence of markov chains with l-lag couplings. In *Advances in Neural Information Processing Systems*, pages 7389–7399, 2019.
- L. Bornn, P. E. Jacob, P. Del Moral, and A. Doucet. An adaptive interacting Wang–Landau algorithm for automatic density exploration. *Journal of Computational and Graphical Statistics*, 22(3):749–773, 2013.
- C. Chimisov, K. Latuszynski, and G. Roberts. Air markov chain monte carlo. *arXiv preprint arXiv:1801.09309*, 2018.
- R. V. Craiu and X.-L. Meng. Perfection within reach: exact mcmc sampling. *Handbook of Markov Chain Monte Carlo*, pages 199–226, 2011.
- R. V. Craiu and X.-L. Meng. Double happiness: Enhancing the coupled gains of l-lag coupling via control variates. *Statistica Sinica*, 32:1–22, 2022.
- J. M. Danby. *Fundamentals of celestial mechanics, Willmann-Bell*, volume 2. 1988.
- C. J. Geyer. Markov chain monte carlo maximum likelihood. *Computing science and statistics: Proceedings of 23rd Symposium on the Interface, Fairfax Station, 1991*, pages 156–163, 1991.
- M. Girolami and B. Calderhead. Riemann manifold langevin and hamiltonian monte carlo methods. *Journal of the Royal Statistical Society Series B: Statistical Methodology*, 73(2):123–214, 2011.
- Q. F. Gronau, E.-J. Wagenmakers, D. W. Heck, and D. Matzke. A simple method for comparing complex models: Bayesian model comparison for hierarchical multinomial processing tree models using warp-iii bridge sampling. *psychometrika*, 84(1):261–284, 2019.
- Q. F. Gronau, A. Heathcote, and D. Matzke. Computing bayes factors for evidence-accumulation models using warp-iii bridge sampling. *Behavior research methods*, 52(2):918–937, 2020.
- A. K. Gupta. Multivariate skew t-distribution. *Statistics: A Journal of Theoretical and Applied Statistics*, 37(4): 359–363, 2003.
- J. Heng and P. E. Jacob. Unbiased hamiltonian monte carlo with couplings. *Biometrika*, 106(2):287–302, 2019.
- M. Hoffman, P. Sountsov, J. V. Dillon, I. Langmore, D. Tran, and S. Vasudevan. Neutra-lizing bad geometry in hamiltonian monte carlo using neural transport. *arXiv preprint arXiv:1903.03704*, 2019.
- P. Jacob, J. O’Leary, and Y. Atchadé. Unbiased markov chain monte carlo with couplings (with discussion). *JR Statist. Soc. Ser. B*, 82:543–600, 2020.
- P. E. Jacob, R. J. Ryder, et al. The Wang–Landau algorithm reaches the flat histogram criterion in finite time. *The Annals of Applied Probability*, 24(1):34–53, 2014.
- S. F. Jarner and E. Hansen. Geometric ergodicity of metropolis algorithms. *Stochastic processes and their applications*, 85(2):341–361, 2000.
- D. E. Jones, D. C. Stenning, E. B. Ford, R. L. Wolpert, T. J. Loredo, C. Gilbertson, and X. Dumusque. Improving exoplanet detection power: Multivariate gaussian process models for stellar activity. *The Annals of Applied Statistics*, 16(2):652–679, 2022.
- A. Kong, P. McCullagh, X.-L. Meng, D. Nicolae, and Z. Tan. A theory of statistical models for Monte Carlo integration (with Discussions). *Journal of the Royal Statistical Society: Series B (Statistical Methodology)*, 65 (3):585–604, 2003.
- F. Liang. Dynamically weighted importance sampling in monte carlo computation. *Journal of the American Statistical Association*, 97(459):807–821, 2002.
- F. Liang. A generalized Wang–Landau algorithm for Monte Carlo computation. *Journal of the American Statistical Association*, 100(472):1311–1327, 2005.
- F. Liang, C. Liu, and R. J. Carroll. Stochastic approximation in monte carlo computation. *Journal of the American Statistical Association*, 102(477):305–320, 2007.
- S. Livingstone, M. Betancourt, S. Byrne, and M. Girolami. On the geometric ergodicity of Hamiltonian Monte Carlo. *Bernoulli*, 25(4A):3109 – 3138, 2019. doi: 10.3150/18-BEJ1083. URL <https://doi.org/10.3150/18-BEJ1083>.
- T. J. Loredo, J. O. Berger, D. F. Chernoff, M. A. Clyde, and B. Liu. Bayesian methods for analysis and adaptive scheduling of exoplanet observations. *Statistical Methodology*, 9(1-2):101–114, 2012.
- X.-L. Meng and S. Schilling. Warp bridge sampling. *Journal of Computational and Graphical Statistics*, 11(3): 552–586, 2002.
- X.-L. Meng and W. H. Wong. Simulating ratios of normalizing constants via a simple identity: a theoretical exploration. *Statistica Sinica*, pages 831–860, 1996.
- R. M. Neal et al. Mcmc using hamiltonian dynamics. *Handbook of markov chain monte carlo*, 2(11):2, 2011.
- B. E. Nelson, E. B. Ford, J. Buchner, R. Cloutier, R. F. Díaz, J. P. Faria, N. C. Hara, V. M. Rajpaul, and S. Rukdee. Quantifying the bayesian evidence for a planet in radial velocity data. *The Astronomical Journal*, 159(2):73, 2020.
- F. Nielsen and R. Nock. On the chi square and higher-order chi distances for approximating f-divergences. *IEEE Signal Processing Letters*, 21(1):10–13, 2013.
- T. P. Papp and C. Sherlock. A new and asymptotically optimally contracting coupling for the random walk metropolis. *arXiv preprint arXiv:2211.12585*, 2022.

- M. D. Parno and Y. M. Marzouk. Transport map accelerated markov chain monte carlo. *SIAM/ASA Journal on Uncertainty Quantification*, 6(2):645–682, 2018.
- E. Pompe, C. Holmes, K. Latuszyński, et al. A framework for adaptive mcmc targeting multimodal distributions. *Annals of Statistics*, 48(5):2930–2952, 2020.
- J. G. Propp and D. B. Wilson. Exact sampling with coupled markov chains and applications to statistical mechanics. *Random Structures & Algorithms*, 9(1-2):223–252, 1996.
- N. Pullen and R. J. Morris. Bayesian model comparison and parameter inference in systems biology using nested sampling. *PloS one*, 9(2):e88419, 2014.
- V. Rajpaul, S. Aigrain, M. A. Osborne, S. Reece, and S. Roberts. A gaussian process framework for modelling stellar activity signals in radial velocity data. *Monthly Notices of the Royal Astronomical Society*, 452(3): 2269–2291, 2015.
- H. Robbins and S. Monro. A stochastic approximation method. *The annals of mathematical statistics*, pages 400–407, 1951.
- G. O. Roberts and J. S. Rosenthal. Coupling and ergodicity of adaptive markov chain monte carlo algorithms. *Journal of applied probability*, 44(2):458–475, 2007.
- U. Şimşekli. Fractional langevin monte carlo: Exploring lévy driven stochastic differential equations for markov chain monte carlo. In *International Conference on Machine Learning*, pages 3200–3209. PMLR, 2017.
- Stan Development Team. *Stan Modeling Language User’s Guide and Reference Manual, Version 2.28*. 2019. URL <http://mc-stan.org/>.
- Stan Development Team. RStan: the R interface to Stan, 2020. URL <http://mc-stan.org/>. R package version 2.21.2.
- N. M. Stein and X.-L. Meng. Practical perfect sampling using composite bounding chains: the dirichlet-multinomial model. *Biometrika*, 100(4):817–830, 2013.
- N. Surjanovic, S. Syed, A. Bouchard-Côté, and T. Campbell. Parallel tempering with a variational reference. *Advances in Neural Information Processing Systems*, 35:565–577, 2022.
- S. Syed, V. Romaniello, T. Campbell, and A. Bouchard-Côté. Parallel tempering on optimized paths. In *International Conference on Machine Learning*, pages 10033–10042. PMLR, 2021.
- S. Syed, A. Bouchard-Côté, G. Deligiannidis, and A. Doucet. Non-reversible parallel tempering: a scalable highly parallel mcmc scheme. *Journal of the Royal Statistical Society Series B: Statistical Methodology*, 84(2):321–350, 2022.
- H. Tak, X.-L. Meng, and D. A. van Dyk. A repelling–attracting metropolis algorithm for multimodality. *Journal of Computational and Graphical Statistics*, 27(3):479–490, 2018.
- C. Villani. *Topics in optimal transportation*. Number 58. American Mathematical Soc., 2003.
- F. Wang and D. P. Landau. Efficient, multiple-range random walk algorithm to calculate the density of states. *Physical review letters*, 86(10):2050, 2001.
- L. Wang, D. E. Jones, and X.-L. Meng. Warp bridge sampling: The next generation. *Journal of the American Statistical Association*, 117(538):835–851, 2022.
- D. Woodard, S. Schmidler, and M. Huber. Sufficient Conditions for Torpid Mixing of Parallel and Simulated Tempering. *Electronic Journal of Probability*, 14(none):780 – 804, 2009. doi: 10.1214/EJP.v14-638. URL <https://doi.org/10.1214/EJP.v14-638>.
- Y. Yan, K. Wang, and P. Rigollet. Learning gaussian mixtures using the wasserstein-fisher-rao gradient flow. *arXiv preprint arXiv:2301.01766*, 2023.
- Y. Yu and X.-L. Meng. To center or not to center: That is not the question—an ancillarity–sufficiency interweaving strategy (asis) for boosting mcmc efficiency (with discussion). *Journal of Computational and Graphical Statistics*, 20(3):531–615, 2011.